1-1-2008

Measuring the mechanical properties of apoptotic cells using particle tracking microrheology

Ahmed El Kaffas
Ryerson University

MEASURING THE MECHANICAL PROPERTIES OF APOPTOTIC CELLS USING PARTICLE TRACKING MICRORHEOLOGY

by

Ahmed El Kaffas

Bachelor of Engineering, Ryerson University, 2005

A thesis

presented to Ryerson University

in partial fulfillment of the

requirement for the degree of

Master of Science

in the program of

Biomedical Physics

Toronto, Ontario, Canada, 2008

AUTHOR'S DECLARATION

I hereby declare that I am the sole author of this thesis.
I authorize Ryerson University to lend this thesis to other institutions or individuals for the purpose of scholarly research.

_____
Ahmed El Kaffas

I further authorize Ryerson University to reproduce this thesis by photocopying or by other means, in total or in part, at the request of other institutions or individuals for the purpose of scholarly research.

_____
Ahmed El Kaffas

Measuring the Mechanical Properties of Apoptotic Cells using Particle Tracking Microrheology

Ahmed El Kaffas
M.Sc., Biomedical Physics, Ryerson University
2008

Abstract

Numerical models developed to study high frequency ultrasound scattering during apoptosis require knowledge of mechanical properties of cells. Particle Tracking Microrheology (PTM) is a technique for studying the mechanical properties of soft materials. By tracking the Brownian movement of particles embedded in a material, its mechanical properties can be extracted. In this thesis, PTM is used to measure the relative changes in the viscoelasticity of apoptotic PC3 cells. PTM was first validated in purely viscous and viscoelastic phantoms. It was found to work well in viscous phantoms, but was limited to only measuring relative changes of the viscoelasticity of viscoelastic materials. After validation, PTM measurements in cells showed that the elastic and viscous modulus increased by over 50 Pa and 20 Pa respectively over the course of the treatment. Preliminary development of another technique known as Two-Point Particle Tracking Microrheology (TPM) is also presented in this thesis.

Acknowledgements

First and Foremost, I wish to express my gratitude to my thesis supervisors Dr. Michael C. Kolios and Dr. J. Carl Kumaradas for introducing me to biomedical physics and cell mechanics and for guiding me every step along the way in developing Particle Tracking Microrheology at Ryerson University.

I would like to acknowledge Arthur Worthington at Ryerson University and Anoja Giles at Sunnybrook hospital for assisting me in both physics and biological aspects of my experiments.

I would like to also acknowledge Hamed Basseri for all the help and commitment with purifying guar and preparations for the cell injection experiments

I also wish to thank my two committee members, Dr. Marcello Papini for helping me in gaining a good understanding of the mechanics of materials, and Dr. Dimitri Androutsos who gave me good insight and food for thought in regards to image processing and analysis. I am also grateful to Dr. John Charles Crocker and Dr. Maria Kilfoil who have guided me immensely in writing code for Two-Point Microrheology.

I would like to thank my fellow students/staff in the Physics department at Ryerson University, Sunnybrook hospital and the Princess Margaret Hospital for their support. Last but not least, I wish to thank my parents and my family for their encouragement and unceasing support.

Dedication

This thesis is dedicated to my loving parents Iman & Nagy, who have always taught me to question and my brother Tarek, for the many wonderful philosophical conversations that keep inspiring our lives.

Table of Contents

List of Tables

List of Figures

Chapter 1

Introduction

1.1 High Frequency Ultrasound for the Detection of Apoptosis

Although the German scientist Carl Voight was the first to describe the principles of apoptosis in 1842, it wasn't until 1972 that John Foxton Ross Kerr (Kerr *et al.,* 1972) first associated the word with what was observed to be a form of programmed cell death, serving as a process for the disposal of cellular debris while reducing damage to organisms. Apoptosis is characterized by a series of biochemical events that lead to nuclear condensation and DNA degradation, and other morphological changes including cellular shrinkage, loss of membrane symmetry, and fragmentation of the cell into apoptotic bodies by a blebbing process (Figure 1.1). Several chemotherapy agents used today to treat cancer aim to induce apoptosis in tumor cells.

High frequency Ultrasound (HFUS) (20MHz - 60MHz) has been used to detect the structural and physical changes in cells undergoing apoptosis. Figure 1.2 shows an increase in ultrasound backscatter of 9-13 dB as cells were treated with cisplatin (Czarnota *et al.,* 1997; Czarnota *et al.,* 1999; Kolios *et al.,* 2004; Kolios *et al.,* 2002). As the ultrasound wavelength approaches the dimensions of cells, as is the case in HFUS, the backscatter becomes more sensitive to cell structures and spatial distributions. This phenomenon can be

potentially used to determine the apoptotic index (the percentage of cells in a volume undergoing apoptosis) and to further quantify patient response to cancer treatment.

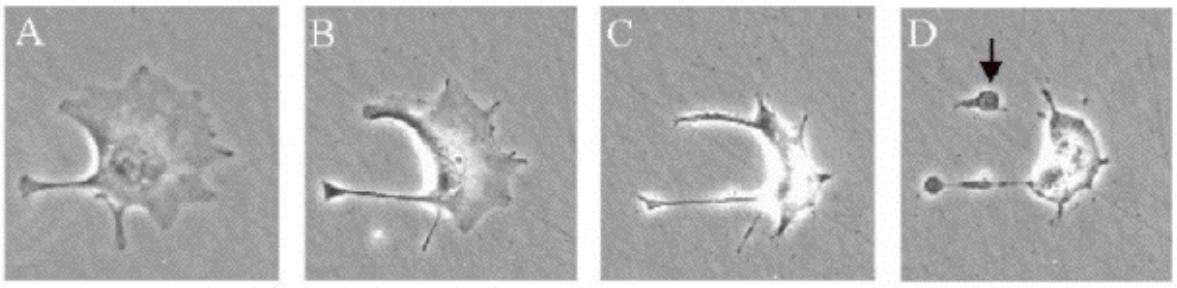

Figure 0.1: Morphological changes of a trophoblast apoptotic cell as captured by time-lapsed microscopy. A) Viable cell before treatment. B) Breakdown of the chromatin in the nucleus leads to condensation of nucleus and shrinkage of the cell. C) Cell continues to shrink as nucleus begins to fragment. At this stage, there is obvious morphological changes in the cell. D) Appearance of membrane blebs or blisters. Apoptotic bodies are also sometimes observed (arrow)[1].

To better understand this phenomenon, theoretical models of acoustic wave scattering from cells have been developed by Falou *et al.* (2006). These models aim to provide a better understanding of how sound waves dissipate in single-cell and multiple-cell ensembles as well as determining which cell structure contributes to HFUS backscatter. However, the mechanical properties of viable and apoptotic cells are not known. The validity of models developed has been questioned due to the lack of available cell mechanical properties. The need for a more complete cell model, which would include the mechanical properties of different structures within the cell, is critical.

[1] www.sgul.ac.uk/depts/immunology/~dash

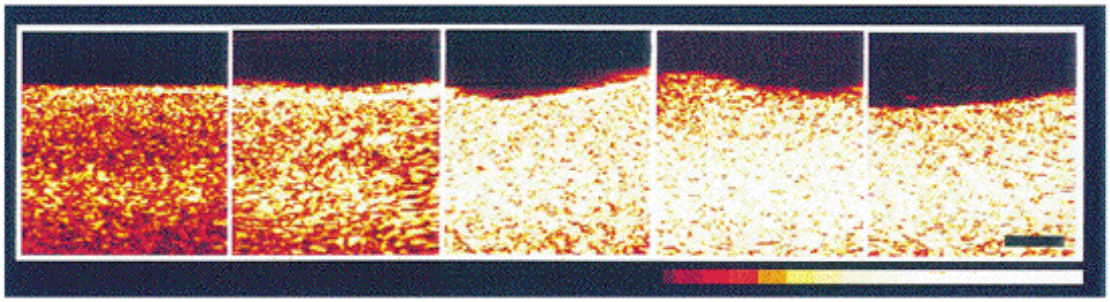

Figure 0.2: Ultrasonic backscatter of acute myeloid leukemia (AML) cells exposed to the chemotherapeutic agent cisplatin after 0, 6, 12, 24 and 48 hrs (from left to right). A bar at the bottom right of the figure indicates the colour map used in this image, the left of the bar indicating the colour that corresponds to pixel values of 0 (lowest intensity) and the right giving the colour that corresponds to a pixel value of 256 (highest intensity). (Czarnota *et al.*, 1999)

1.2 Cell Mechanics

The cell is considered to be a basic component of life and is the focus of most biological and medical research. Cells are highly dynamic entities, which constantly remodel their internal structure in response to chemical and physical stimuli, which in turn affects their mechanical properties (Jiang *et al.,* 2006). Furthermore, structural heterogeneity within the cell complicates measuring these properties (see Figure 1.3 displaying the many structures of the cell). Therefore new techniques to probe the mechanical properties of cells have been recently developed.

Cell mechanical properties differ at different length and time scales. Cell mechanics are largely determined by the cytoskeleton, a biopolymer network made up of filamentous actin, intermediate filaments and microtubule. Several investigators have attempted to measure the mechanical properties of the cytoskeleton as either a reconstituted polymer network *in vitro* (mimicking the cell's cytoskelton), or in living cells (Gardel *et al.,* 2006; Gisler & Weitz, 1999; Mason *et al.,* 2000; Van Citters *et al.,* 2006; Xu *et al.,* 1998).

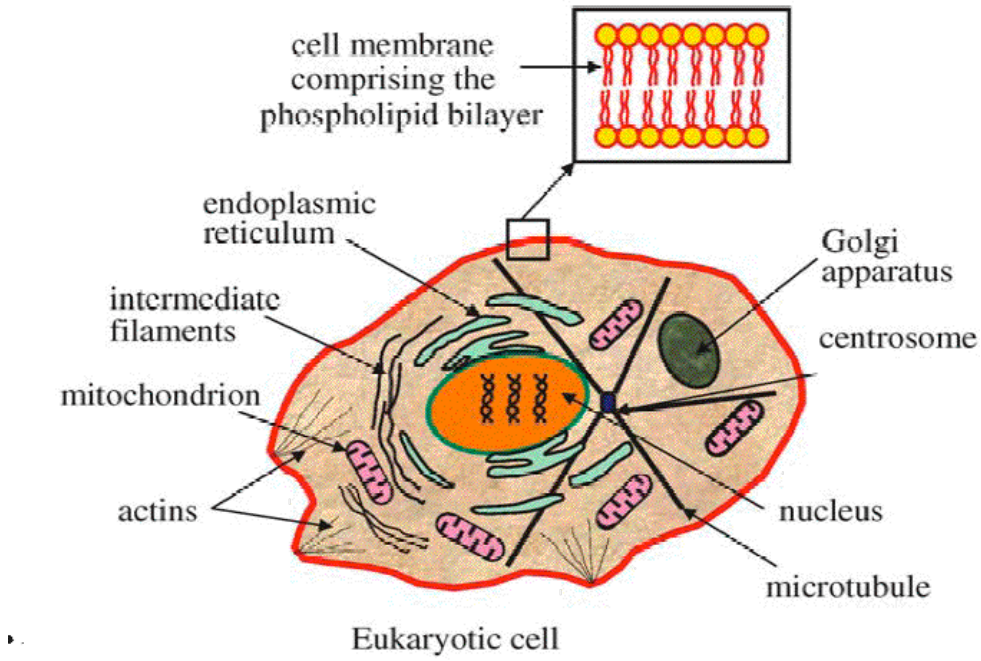

Figure 0.3: Figure of a cell displaying the various components of the cell that make up its heterogeneity (Lim, *et al.*, 2006)

Investigators have shown that cells have both an elastic and a fluid component in their mechanical properties. Kasza *et al.* (2007) gives a good review of research on cell mechanics. They have demonstrated that cells are more similar to gels, although they slowly deform under steady stress for an indefinite time. These characteristics are common in viscoelastic media, where the elastic modulus depends on the degree of applied or internal stress.

Over the last 3-4 years, several groups have attempted to develop mathematical models of a cell (for a comprehensive review see Lim *et al.* (2006)). The highly heterogeneous structure of the cell makes modeling its mechanical properties a challenging task. Kasza *et al.* (2007) state that a complete model should "account for all components that contribute to the mechanics of the cell, as well as the interactions between these components

that result in the full 'system' behaviors". Models are often developed to account for properties at specific time or length scales, and tend to describe cells as either a viscoelastic continuum, a network of discrete mechanical elements, or a combination of viscoelastic fluids. For each of these models, there exists experimental observations, which either agree or disagree with the model (Pelling *et al.*, 2008).

Physiological processes cause the cell to constantly restructure itself, inducing time dependent changes in its mechanical properties. By studying these mechanical changes, researchers have hoped to better understand cellular processes as to help optimize biomedical treatments and assays (Pelling *et al.,* (2008); Kole *et al.,* (2005); Kasza *et al.,* (2007)). Determining the mechanical properties of cells, although challenging, is therefore very interesting and important.

1.2.1 Measurement of Cell Mechanical Properties

The study of cell mechanics has been a growing field for the past 150 years. Researchers are motivated to develop an understanding of mechanical and structural changes occurring in cells in various biological and biochemical processes, such as cell migration and metastasis, adherence, or simple response to various cellular environments. The development of techniques for studying the mechanical properties of cells has been challenging. The fundamental approach behind these newly developed methods is to measure cell deformations as a response to a force. A consensus has developed that cells are soft viscoelastic materials on a large scale but increasingly heterogeneous at smaller length scales ($< 1\mu m$). As a whole, the cell is typically considered to be predominately viscous at lower

frequencies and more elastic at higher frequencies (Tseng *et al.,* 2002), but there is no consensus at which frequency this transition occurs.

"Cell poking", which involves probing the cell with calibrated micro-needles, was among the first methods used to measure cell mechanics. Other techniques such as micropipette aspiration, deformation with micro-plates, atomic force microscopy, optical tweezers and magnetic traps were later developed (Gardel *et al.,* 2006). These techniques all involve the measurement of a deformation in response to an active force. Although multiple laboratories around the world have now successfully used these techniques for measuring the mechanics of cells, many questions regarding the meaning and accuracy of measurements by these techniques are still being asked today (Pelling *et al.,* 2008), though recent techniques have yielded a more unified view of the cell as a whole.

1.2.2 Microrheology for Measuring Cell Mechanics

Microrheology collectively refers to a family of recently developed techniques to measure the viscoelastic properties of complex fluids and soft materials with relatively high temporal and spatial resolution (Waigh, 2005). It uses Brownian motion to assess viscoelasticty. By tracking the motion of micron-sized particles embedded in a material, mechanical properties can be determined. Active microrheology, such as the techniques named in the previous section, uses external forces to manipulate probe-particles, while passive methods simply allow the particles to be driven by the thermal energy of the material. Passive methods have an advantage over active methods since no large strain or stress is applied to the cell and a linear response can be measured directly. This is particularly useful in soft materials and complex fluids where even a small-imposed strain can cause reorganization of structure

within the material and thus change its viscoelastic properties (e.g., strain hardening or shear thinning, Waigh, 2005).

In this thesis, Particle Tracking Microrhelogy (PTM) was used to study the mechanical properties of viable vs. apoptotic cells. PTM consists of tracking the Brownian motion of tracers embedded in a material, and extracting mechanical properties of the material using mathematical analysis. The technique has previously been applied on a variety of complex fluids and gels (polymers, colloids and biological materials); Waigh (2005) provides a good review of the non-biological use of PTM . Several groups have measured the mechanical properties of F-actin (polymerized actin protein) gels using PTM (Mason *et al.,* 2000; Crocker *et al.,* 2000; Valentine *et al.,* 2001; Valentine *et al.,* 2003; Gardel *et al.,* 2006). The interest in F-actin arises from the fact that it is the main constituent of the cell's cytoskeleton, giving the cell's cytoplasm its elastic properties. Particles, already present or inserted in cells via endocytosis or microinjection, have been used to study local and bulk mechanics of cells. Kole *et al.,* (2005) were amongst the first to apply the technique as a tool to measure intracellular mechanical properties. Their initial experiments supported the hypothesis that high levels of heterogeneity are present within the cell.

Recently, PTM has been used to evaluate the mechanics of various biological systems, varying from DNA solutions (Chen *et al.,* 2003), actin filaments (Crocker *et al.,* 2000; Gardel *et al.,* 2006; Mason *et al.,* 2000; Valentine *et al.,* 2001; Valentine *et al.,* 2003) to stress caused by expanding tumor systems (Gordon *et al.,* 2003) and the mechanics of human cystic fibrotic sputum (Dawson et al., 2003). Excellent reviews of the application of PTM to biological systems are available (Gardel *et al.,* 2005; Waigh, 2005; Weihs *et al.,* 2006). Apart

from *in-vitro* systems, Tseng *et al.*, (2002a) developed a spatial mapping of the mechanical properties of Swiss 3T3 fibroblast cells. Their work showed that the lamella (0.25-1μm away from nucleus) tends to be stiffer than the perinuclear region (0-0.25 μm away from the nucleus). They concluded that the cytoplasm of fibroblasts generally behaves like a stiff elastic material when deformed rapidly and like a soft viscous liquid when deformed slowly. Their work also shows that cells microinjected with α-actinin (a protein which cross-links F-actin polymers) are stiffer and yet mechanically more heterogeneous than Swiss 3T3 viable control cells. Work by Daniels *et al.* (2006) studied the mechanics of developing Caenorhabditis elegans embryo cells. They reported that, unlike differentiated cells, no elasticity is detected in the cytoplasm of these embryos. PTM measurements in the intranuclear region of the cell have revealed its predominantly elastic nature in contrast to the cytoplasm, which tends to be more viscous (Tseng *et al.,* 2004). Kole *et al.,* (2005) showed, through the use of PTM, that the cytoplasmic reorganization produced by cell motility results in the stiffening of both the lamella and perinuclear region of the cell. Finally, Tseng *et al.,* (2002b) showed that the ensemble averaged mean square displacement of an embedded particle increases in the lamella and decreases in the perinuclear region of the cell (indicating that the lamella softens while the perinuclear region stiffens) when cells are exposed to LPA, a small molecule that re-organizes the actin filaments (cytoskeleton) of the cell. These are still however several limitations of PTM that make the results difficult to interpret. The limitations will be discussed in Chapters 2 and 3.

Two-Point Particle Tracking Microrheology (TPM) was developed as an extension to PTM. It extracts the mechanical properties from the cross-correlation of the displacements of

pairs of particles. The Brownian motion of particles yields only the local mechanical properties of materials on the length scale of the particle. TPM was developed as a tool to measure bulk mechanical properties of materials at length scales greater than the radius of the particle-probes in cases where the particle-probes are much smaller than the length-scale of heterogeneity of the material. Crocker *et. al*., (2000), who developed the technique, showed that TPM more accurately measures the bulk shear modulus in guar solutions when compared to PTM. TPM has also been used to measure the mechanics DNA solutions and F-actin systems (Chen *et al.*, 2003; Crocker & Hoffman, 2007a; Lau *et al.,* 2003). Lau *et al.,* (2003) were first to use TPM on cells showing that the cytoplasm is a continuum with its viscoelasticity changing as a function of lag-time. Crocker *et al.* (2000) provides a good review of TPM.

1.3 Hypothesis and Specific Aims

I hypothesize that PTM can be used to detect changes in the mechanical properties of cells treated with a chemotherapeutic agent that induces apoptosis. It is assumed that such measurements will yield only an average of the local mechanical properties of healthy and apoptotic cells. To validate my hypothesis, it is essential to first develop and validate PTM in well controlled viscous and viscoelastic samples. To do so, microrheological measurements were performed on glycerol/water and guar/water solutions. Glycerol is a linear Newtonian fluid, which has only a viscous component and is therefore ideal for the initial calibration of the technique for viscous measurements. Guar is a naturally occurring neutral polysaccharide extracted from guar gum. A small amount of the powder dramatically changes mechanical properties of water, forming aggregates due to the random associations of guar molecules. It

is therefore an ideal inhomogeneous soft material for viscoelastic measurements. PTM was then used to measure the average mean square displacement (MSD) of microinjected particles in cells, from which the viscoelastic modulus is extracted at different frequencies. Preliminary attempts to develop and validate TPM in guar and glycerol solutions are presented in the results section of this thesis. To my best knowledge, this is the first time that PTM is used to study mechanical changes in cancer cells undergoing chemotherapeutic treatment. This thesis provides new insight on the nature (qualitative and quantitative) of mechanical property changes that treated cells undergo during apoptotic cell death. This work will also aid in the development of more accurate theoretical models of ultrasound scattering by cells.

Chapter 2

Theory

2.1 Brownian Motion

Brownian motion is a mathematical model that describes the random motion (or random walk) of particles embedded in a system of molecules. It is in essence the backbone of PTM. This motion can be quantified and further used to study the mechanical properties of materials. In this chapter, Einstein's mathematical model of Brownian motion is derived and related to the viscosity of the material in which particles are embedded. The concept of viscoelasticity is then explained. Finally, the quantified motion of a particle embedded in a complex material is related to the viscoelasticity of the material surrounding the particle.

2.1.1 History of Brownian Motion

In 1765, Jan Ingenhousz became the first scientist to record his observations of the irregular, or random, motion of carbon dust in alcohol. Less than a hundred years later, in the late 1820s, Scottish botanist Robert Brown became interested in this irregular motion. He had observed it while looking at clarika pollen in water under the newly invented microscope. Having read of other testimonies to this motion, his observations did not strike him as a surprise. It was a common belief at the time among other botanists that this movement represented the essence of life. Brown doubted this notion.

To show that the irregular movement of clarika pollen did not represent the essence of life, he conducted an experiment, where pollen was stored in alcohol for 11 months. The fact that he could still see the motion made the life-essence theory unlikely, as alcohol was known to preserve by killing off life. Furthermore, he observed similar motion in experiments conducted with powdered rock, metals and carbon particles. These experiments were logged in his "Brief Account of Microscopical Observations", published in 1828 (Brown, 1828). Although Robert Brown was unable to give an adequate explanation as to the nature of the motion observed, he is credited with the discovery of what was later to be known as "Brownian motion".

With the development of the kinetic theory of gases during the mid-nineteenth century, scientists began to question the effect of excited gas or liquid molecules on submerged particles. Ignace Carbonelle, Joseph Delsaulx and William Ramsey put together the first qualitative description of the Brownian motion of solid particles in a liquid, and proposed that the irregular motion of a particle was due to constant bombardment by molecules belonging to the surrounding medium. They speculated that large particles would also be subjected to this bombardment on all sides equally, causing the forces to cancel out; in such a situation, no Brownian motion would be observed. On the other hand, smaller particles would be bombarded on all sides causing an imbalance, which would then cause a biased movement of these particles as shown in Figure 2.1. Predicting the trajectory of these movements is impossible and appears to be a random wiggle, which grows in area with time.

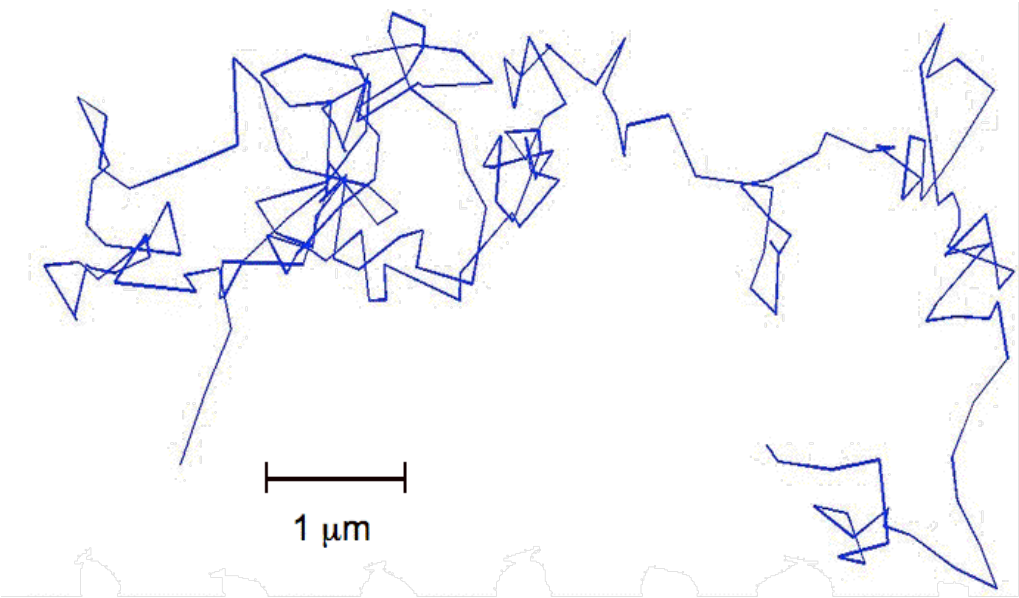

Figure 0.1: Track of the random walk or Brownian motion of a 0.2 μm particle in 90% w/w glycerol-water solution.

Seven principal features of Brownian motion were noted by scientists studying this phenomenon (Haw, 2002):

- Movement is irregular and consists of both, straight line movements and rotations of the particles
- The Brownian Motion of each particle is independent of all other particles surrounding it, even at close range (as long as there is no collision)
- The smaller the particle (relative to particles/molecules/atoms surrounding it), the more vigorous the motion is
- The chemical makeup and physical density of the particles has no effect on the motion

- The motion is more vigorous in less viscous liquids
- The motion is more vigorous at higher temperatures
- The motion continues indefinitely if effects such as evaporation are eliminated. (This is supported by the observation of the motion in waterborne suspensions trapped for thousands of years in quartz (Haw, 2002)).

At that time, the atomic nature of matter was a controversial subject and different atomic theories were still being debated. Scientists could only agree on the usefulness of the atomic model, but no physical proof of the atoms existence was available. Albert Einstein attempted to prove the existence of atoms for his Ph.D. research (Einstein, 1956). He began by developing the first mathematical model of Brownian motion. Einstein and Marian Smoluchowski (a Polish scientist, and a pioneer of statistical physics) observed that, if the kinetic theory of fluids was right, then molecules of water would constantly move at random. Therefore a small particle would receive a random number of impacts of random strength and from random directions in any short period of time. This random bombardment by the molecules of the fluid would cause a sufficiently small particle to move in exactly the way described by Brown and others.

Einstein formulated a mathematical model of Brownian Motion, which he used to explain and argue for the existence of atoms, basing his work on the assumption that atoms do exist, from which he attempted to understand and predict the motion of other entities (such as particles) submerged in a collection of atoms. Einstein's first attempts at explaining the observed motion were aimed at describing the diffusion of multiple particles in a fluid

and how the molecules of this fluid would cause the particles to counteract gravity to some extent before settling to the bottom. He predicted that such a phenomenon would mean that there would always be a (even small) concentration of these particles at the top of the liquid, and that they would not all settle to the bottom of the medium.

His approach yielded good results because he concentrated on the average condition of a large number of particles so that the behaviors of individual particles became blurred. This enabled him to predict the concentration of particles in a given region without knowing where those particles had been or will be. Jean Perrin then carried out experiments to test the new mathematical models in 1909; the results of his published work finally put to an end the two thousand year question about the reality of atoms and molecules. In the 1920s, Norbert Wiener developed a mathematical model for predicting a probability map for the position of a single particle after a given time; this type of movement is now known as "random walk", and falls under the greater science of probability, a science that studies random influences on systems. In Brownian motion, the variable under observation is the particle position and the influencing system is the fluids' molecules. Today random walks are used in various fields such as market analysis, urban planning, computer design networks, and rheology and microrheology (Haw, 2002).

2.1.2 Einstein's Model of Brownian Motion

Einstein investigated how the process of diffusion of a solute depends on the mobility of the dissolved substance in a solvent and on the osmotic pressure in the solution as a whole. This yields an expression linking the diffusion–coefficient to the viscosity of the solvent and the diameter of the solute molecules. His analysis assumes that the solute molecules are much

larger than those of the solvent, from which he was able to relate the diffusion term to the displacement of the particle caused by the irregular random motion (Einstein, 1956; Haw, 2002).

To better understand his investigation, one can envision a scenario such as in Figure 2.2, where a solute covers the tiny area of *dA* (red) and is surrounded by solvent molecules (orange). The osmotic pressure difference acting on the solute is $p - p'$.

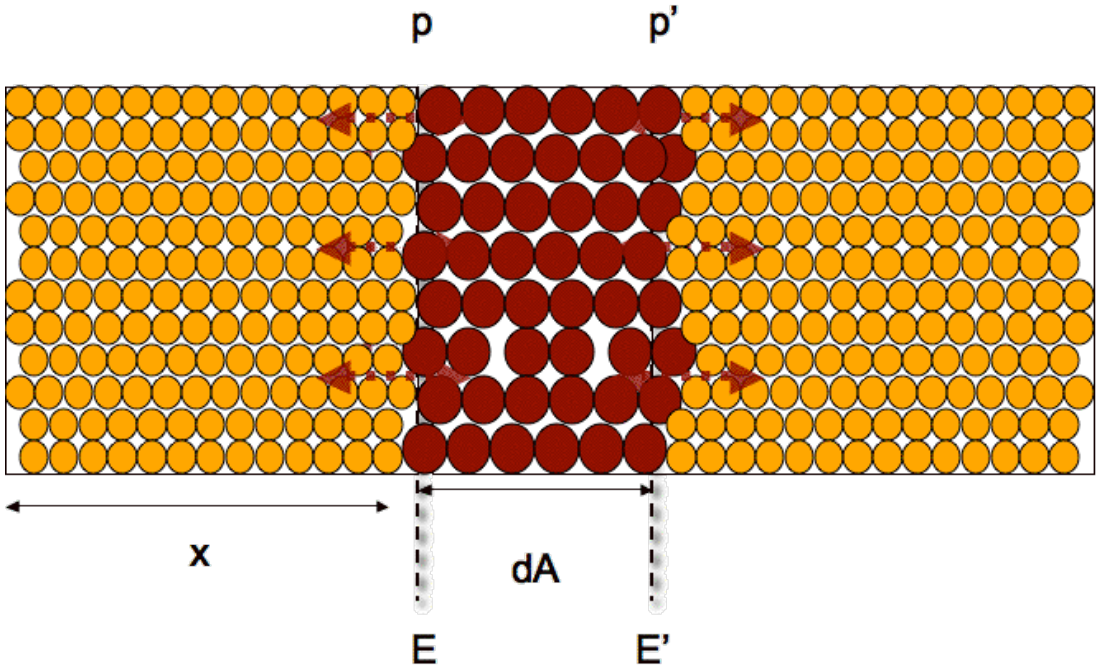

Figure 0.2: The area dA contains a solute which is about to diffuse into the surrounding solvent. The molecules of the solute are larger than those of the solvent as seen. The pressure at the boundaries is p and p'. Einstein used a similar diffusion model to derive the Brownian motion model.

K can be defined to be the osmotic pressure acting on a unit area of the solute

$$K = \frac{p - p'}{dA} = -\frac{dp}{dA}. \qquad [1]$$

The ideal gas law can also be used to describe pressure,

$$p = RTc, \qquad [2]$$

where R is the universal gas constant, T is the absolute temperature in Kelvin and c is the number of moles of molecules per unit volume. Combining equations [1] and [2] yields

$$K = -RT\frac{dc}{dA}. \qquad [3]$$

From the active force induced by K on a molecule, one can calculate a velocity, u, as follows

$$u = \frac{K}{\beta}, \qquad [4]$$

where β is a constant known as the frictional resistance of the molecule. If the solute molecules (or particles) are large (in comparison to the solvent molecules) and are spherical, then this constant can be described by Stokes' hydrodynamic formula

$$\beta = 6\pi a\eta, \qquad [5]$$

where a is the radius of the solute molecules and η is the viscosity of the solvent. Furthermore, if there are cN molecules in the volume in total, where N is Avogadro's number, then K will be distributed over all molecules in the solute. This yields the following velocity for each individual solute molecule

$$u = \frac{K}{cN\beta}. \qquad [6]$$

By combining equation [3] and [4], the following is obtained:

$$uc = -\frac{RT}{N\beta}\frac{dc}{dA}. \qquad [7]$$

The left side of this equation represents the number of moles of the dissolved substance carried per second by diffusion through a unit area of the cross section. The multiplier of $\frac{dc}{dA}$ is known as the diffusion coefficient *D*

$$D = \frac{RT}{N\beta}. \qquad [8]$$

In the case where Stokes' hydrodynamic equation applies, equation 8 becomes

$$D = \frac{RT}{N6\eta\pi a}. \qquad [9]$$

Equation 9 demonstrates the relation between *D*, the viscosity of the solvent and the radius of the solute molecules. $\frac{R}{N}$ is also known to be Boltzmann's constant, $k_{b,}$, where

$$D = \frac{k_b T}{6\eta\pi a}. \qquad [10]$$

This relation soon came to be known as the Stokes-Einstein relation (Einstein, 1956).

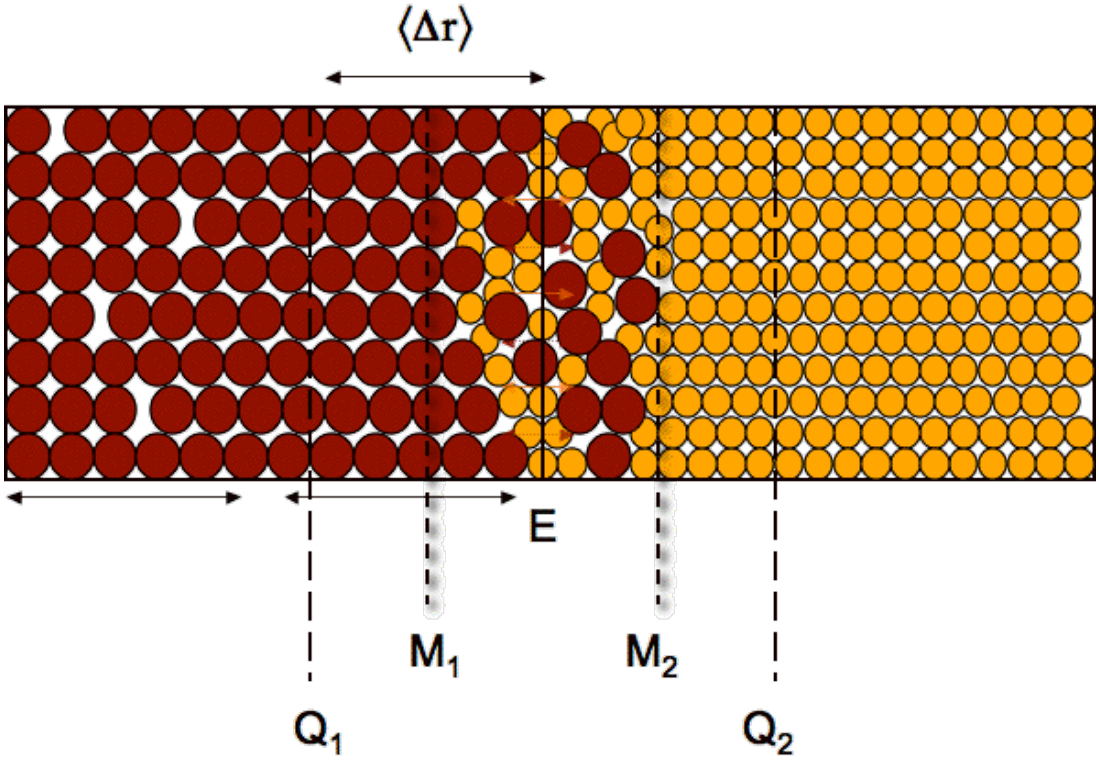

Figure 0.3: A solute diffuses into a solvent left to right. E, Q_1, Q_2, M_1 and M_2 are used as reference lines to help in the derivation of the Brownian motion model. The idea is to study the number of solute molecules crossing E within the time frame τ.

One can also derive an equation relating the diffusion coefficient to the observed displacement of a particle under the influence of Brownian motion. Let us examine solute molecules diffusing into a solvent (left to right) as seen in the tube-like container of Figure 2.3.

If $\langle \Delta r \rangle$ is assumed to be the average distance traveled along the x-axis by a molecule in a time interval τ, a molecule will need to be situated between Q_1 and E to cross over to the other side. In other words, it needs to be within a distance $|\langle \Delta r \rangle|$ from E. Due to the random

nature of Brownian motion, it is assumed that only half of the molecules on either side of E will move towards E.

If c_1 is the concentration of molecules at the middle layer M_1, and c_2 is the concentration of molecules between at the middle layer M_2, then $\frac{1}{2}\langle \Delta r \rangle (c_1)$ is half the number of molecules on the left side of E which could potentially cross E and $\frac{1}{2}\langle \Delta r \rangle (c_2)$ is the number of molecules on the right side that will cross E. Based on this assumption, the number of molecules that will cross from left to right in the time-frame τ, is

$$N_{12} = \frac{1}{2}\langle \Delta r \rangle (c_1 - c_2). \qquad [11]$$

By denoting x to be the distance from M_1 to M_2 in Figure 2.3 (also equal to $\langle \Delta r \rangle$), the following can be obtained:

$$\frac{(c_2 - c_1)}{\langle \Delta r \rangle} = \frac{dc}{dx}. \qquad [12]$$

Combining equation [11] and [12] yields the quantity of the substance which diffuses in time τ

$$N_{12} = -\frac{1}{2}\langle \Delta r \rangle^2 \frac{dc}{dx}. \qquad [13]$$

This quantity can also be expressed in units of time as

$$N_{12} = -\frac{1}{2}\frac{\langle \Delta r(\tau) \rangle^2}{\tau}\frac{dc}{dx}. \qquad [14]$$

This equation similar to equation [7], where the diffusion coefficient is

$$D = \frac{1}{2}\frac{\langle \Delta r(\tau) \rangle^2}{\tau}. \quad [15]$$

The diffusion coefficient is here related to the displacement of particles within a lag time

$$\langle \Delta r(\tau) \rangle = \sqrt{2D\tau}. \quad [16]$$

Adding a dimension term, *n*, yields the following,

$$\langle \Delta r(\tau) \rangle = \sqrt{2nD\tau}, \quad [17]$$

where *n* changes to 2 when the displacement is observed in 2 dimensions, and to 3 in 3 dimensions (Einstein, 1956).

By measuring the motion of single molecules or particles diffusing in a solvent, it is then possible to extract the solvent's viscosity when equations [10] and [17] are combined:

$$\eta = \frac{nk_bT\tau}{3\pi a\langle \Delta r(\tau) \rangle^2}. \quad [18]$$

2.2 Viscoelasticity

Viscosity is the property of a material describing its resistance to flow as a fluid when a shear stress (stress is the average amount of force exerted per unit area) is applied, whereas elasticity can be thought of as a measure of deformation in a solid in response to a stress (otherwise known as a strain). A viscous system (such as Newtonian fluids: e.g. water, oil or glycerol) will always loose its shape and dissipate energy in response to a stress through viscous flow, whereas a purely elastic system (such as a simple solid: e.g. rubber band or a bouncing ball) will store energy and return to its original shape, providing a spring-like effect, once the stress is removed (that is if the shear stress applied does not exceed a

threshold intrinsic to the given material that would permanently alter its shape) (Gardel *et al.,* 2005). A complex material, which exhibits both viscosity and elasticity, is known as a viscoelastic material. The study of the mechanical properties of solids and fluids is known as rheology, defined as the study of deformation and flow of simple and complex systems in response to an applied stress or strain at different time scales (Phan-Thien, 2002).

To better understand viscoelasticity, one should first understand two phenomena common to viscoelastic materials: *stress relaxation and creep*. The stress relaxation function $G(t)$, is the ratio of the instantaneous stress $\sigma(t)$ to an applied strain ε_0

$$G(t) = \frac{\sigma(t)}{\varepsilon_0}, \qquad [19]$$

while the creep function $J(t)$, is the ratio of the instantaneous strain $\varepsilon(t)$ to an applied stress σ_0

$$J(t) = \frac{\varepsilon(t)}{\sigma_0}. \qquad [20]$$

In the field of rheology, the stress relaxation and creep functions are of great interest and are found by applying a load on the material under study and measuring the resulting stress or strain. Various models of viscoelasticity have been developed: Maxwell, Voight and Kelvin were the first to attempt to do so by creating block diagrams based on springs and dashpots. Springs were used to model the elastic nature of a system while the dashpot would represent its viscous nature. While disputes arose in choosing how to place these blocks (series or parallel, how many, order) for different materials, such models eventually evolved into

complicated systems and became hard to deal with mathematically (Fung, 1993; Humphrey, 2004).

Eventually Ludwig Boltzmann came up with a more commonly used model. He proposed that it was important to keep track of the stress/strain response from a load over time. Since relaxation tests are more common, Boltzmann based his model of viscoelasticity on the relaxation function. In his model, he showed that the complex shear modulus (also known as the viscoelastic modulus or the bulk modulus), a measure of viscoelasticity, could be expressed as

$$G^*(\omega) = G_1(\omega) + iG_2(\omega), \qquad [21]$$

where G_1 and G_2 are known as the storage (elastic) and loss (viscous) modulus respectively.

Boltzmann's complex shear modulus is an adequate model of viscoelasticity commonly used today to measure mechanical properties of materials and fluids as a function of frequency. The shear modulus can be measured using a commercial tool known as a rheometer. By applying a force on a small sample of interest, the rheometer is able to measure resulting strain or stress at frequencies up to 10^2 Hz. Typically, specialized tests have to be done before rheometer measurements to determine the range of frequencies and maximum amplitude of force for which the material remains linear. Overall, rheological measurements have proven their validity and given valuable insight into characterizing the mechanical response of various materials and fluids including colloidal suspensions, polymer solutions and gels, emulsions and surfactants (Gardel et al., 2005).

2.3 Microrheology

Microrheology is a family of recently developed techniques, which aims to study the mechanical properties of soft materials at a micron and sub-micron scales. Although conventional rheology requires relatively large quantities of a sample for measurements, microrheology is able to extract viscoelastic quantities using minute samples (in the range of μl for viscoelastic fluids). Moreover, rheometer measurements provide only bulk measurements, while microrheology has been shown to measure both local and bulk mechanical properties.

Microrheology techniques can be classified into two categories: passive and active (Figure 2.4). In active microrheology, a controlled load is used to apply a stress locally to a material and the resulting deformation is then measured. The deformation measurements are then used to quantify the viscoelasticity of the material. Typically, active loads are manipulated using electric or magnetic fields, or micromechanical forces.

Passive microrheology, however, involves utilizing the inert thermal energy of a material to cause a probe to move (Brownian Motion). The total movement (or diffusion) of the probe can then be measured and related to the system's mechanical properties. Although active techniques allow for rheological measurements for a broader range of frequencies, passive microrheology guarantees that measurements do not cause damage to the material, applying forces on the order of only a few pico-newtons. Passive microrheology is minimally invasive if the particle probes do not affect the mechanical properties of the system. Another advantage to passive microrheology is the simplicity of the method and its implementation of the technique. While active microrheology may require sophisticated instrumentation,

passive methods can be as simple as tracking the motion of micro-particles placed or already present in the material under study.

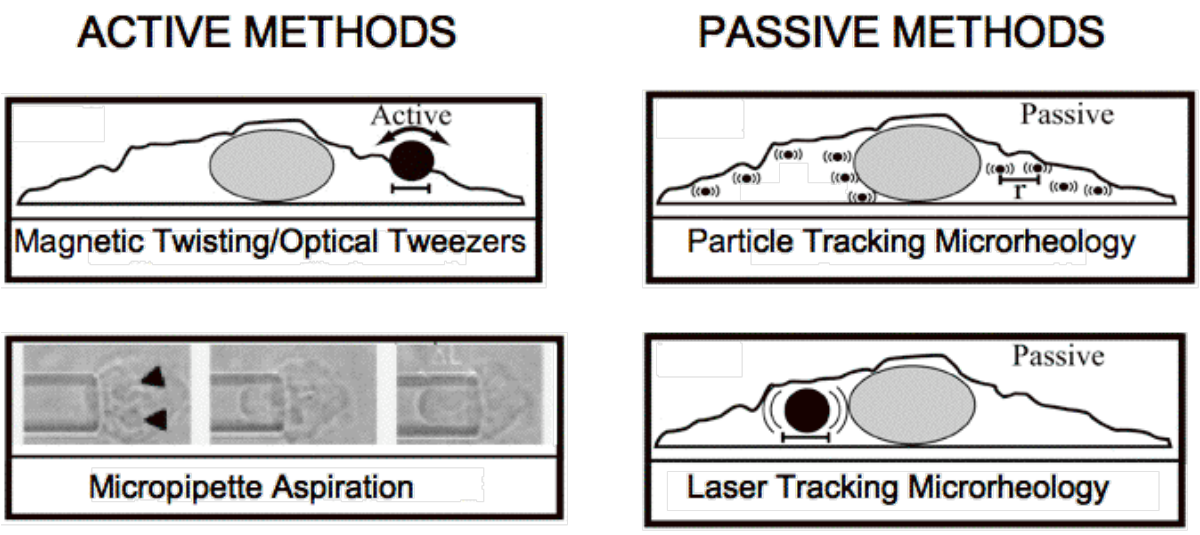

Figure 0.4: Active Microrheology refers to applying a controlled force on a material and measuring a resulting deformation while passive microrheology probes the material using its thermal energy. Top/left: Uses magnetism or optical tweezers to cause a probe to move on the surface of the cell. Bottom/left: applies a suction pressure on the surface of the cell. Top/right: Particle tracking microrheology as described in this thesis. Bottom/right: a passive method where particle movement is detected by a laser. (Adapted from Hoffman *et al.*, 2006)

2.3.1 Particle Tracking Microrheology

Passive microrheology measures the Brownian motion of particles to extract mechanical properties at small scales. The stress imposed on the material under study originates from the stochastic collision of the molecules of the system onto the probe. This stochastic collision is driven by the thermal energy of the system, k_bT. In Particle Tracking Microrheology (PTM), miniscule particles (in the range of 1μm to 100 nm) are inserted in a material. Magnified movies of the Brownian motion of the particles are then taken with a video camera mounted to a microscope.

By using specialized image processing software and tracking routines, it is then possible to track the movement of these particles at a sub-pixel accuracy of 10 nm (Crocker et al., 1996). Tracks can then be used to compute the mean square displacement (MSD), $\left\langle \Delta r^2(\tau) \right\rangle$, for each individual bead and then, using a generalized form of the Stokes-Einstein equation (equation 18), used to extract mechanical properties. The theoretical frequency upper limit on PTM has been reported to be around 100 kHz due to inertial effects (Gardel et al., 2005; Levine et al., 2000). The practical frequency upper limit ranges around ~80 Hz when using a CCD camera, depending on the frame rate of capture and resolution choice. The lower limit depends on how long particles remain within the plain of focus of the microscope.

PTM requires that the material be "soft enough" so that particles may be driven by the thermal energy of the material, and that the material is also translucent, so that the particles can be seen under the microscopic. Currently, the range of measurable viscoelastic moduli is between 10 μPa and 1 Pa. PTM has the advantage that single particles can be analyzed individually, yielding localized measurements, or averaged, giving the average mechanical properties of a heterogeneous material. Techniques have been developed to map spatial and temporal variation in mechanical properties (Valentine *et al.,* 2001).

Equation [18] will be valid in purely viscous fluids where the Mean Square Displacement (MSD) will scale linearly on a log scale with the lag-time τ. In more complex fluids, this relationship will not hold and the MSD will scale differently, through the proportionality constant τ^{α} (Mason *et al.,* 1995). The new, non-linear, relationship can be expressed as follows:

$$\left\langle \Delta r^2(\tau) \right\rangle \propto \tau^{\alpha} \quad [22]$$

Figure 2.5 illustrates various scaling of the MSD for different proportionality constants on a log-log graph. If in a purely viscous material, $\alpha = 1$, the MSD scales linearly with the time-scale. In a viscoelastic material, $0 < \alpha < 1$. In purely elastic materials, the particle is confined and $\alpha = 0$. In this case, the Stokes-Einstein relation becomes

$$\left\langle \Delta r^2(\tau \to \infty) \right\rangle = \frac{k_b T}{\pi a G_1}, \quad [23]$$

where G_1 is the storage modulus of the complex shear modulus. In super-diffusive cases, often the probes move due to active forces (and not just diffusion), $\alpha > 1$.

In many systems where tracers are much smaller than the length scale of heterogeneity, a plateau will be observed at higher lag times, because of the particle's confinement in a pore or a mesh of the material. These power law relations can provide valuable insight into the materials mechanical nature and the particle's surrounding environment. For example, intracellular active motors can cause an injected tracer to move non-randomly throughout the cytoskeleton, resulting in super-diffusion. In such a case, depending on the nature of the study, tracers expressing super-diffusion can be omitted.

The complex shear modulus can be related to the Mean Square Displacement (MSD) of the Brownian motion by generalizing the Stokes-Einstein Equation (equation [18]) to account for elasticity as well as viscosity, in which case the viscous term becomes $G^*(\omega) = G_1 + G_2 i$, where the real component is the storage modulus (elastic) and the

imaginary component represents the loss modulus (viscosity). This new equation is named the Generalized Stoke-Einstein Equation and is expressed as follows:

$$G^*(\omega) = \frac{k_b T}{\pi a i \omega \Im_u \left\langle \Delta \tilde{r}^2(s) \right\rangle}, \qquad [24]$$

where $\Im_u$ is the Unilateral Laplace transform (a Laplace transform generalized for a complex frequency). The equation was originally derived on an ad-hoc basis to analyze the thermal fluctuation spectrum of probe spheres (Levine *et al.,* 2000; Mason, 2000; Mason *et al.,* 2000; Mason *et al.,* 1995), and later placed on firmer theoretical foundations by Levine et al. (2000).

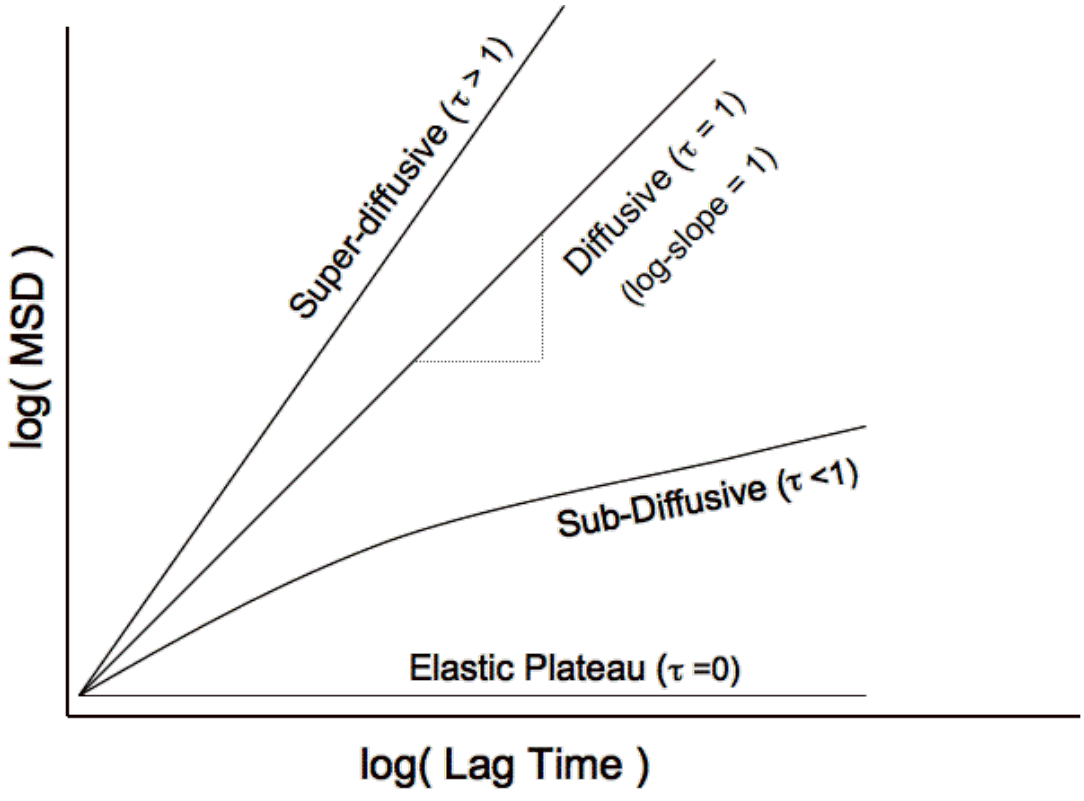

Figure 0.5: MSD vs. Lag-Time trends which represent different kinds of diffusions. The local (at a given lag-time) slope of these lines is then used in computing the complex shear modulus of the material.

Note however that the Unilateral Laplace transform theoretically spans from zero to infinity, which cannot be achieved in practice due to frequency limitations of PTM. Numerous numerical methods have been introduced to overcome this problem (for a review see Waigh (2005)). A simpler algebraic estimation method introduced by Mason (2000) was used in this thesis. In summary, the method estimates the complex shear modulus algebraically by finding the local log-slope (or log-derivative) of the MSD around each time-scale individually. A line is then fit which extends to both sides of the chosen time-scale point. This yields a smoothed approximation of the MSD, from which the slope α (which is also the logarithmic derivative) can be taken:

$$\alpha(\tau) \equiv \frac{d \ln \left\langle \Delta \vec{r}^2(\tau) \right\rangle}{d \ln \tau}. \qquad [25]$$

This slope can then be used to compute the magnitude of the shear modulus as follows

$$\left|G^*(\omega)\right| = \frac{k_b T}{\pi a \Gamma(1+\alpha(\omega)) \left\langle \Delta r^2(\frac{1}{\omega}) \right\rangle}, \qquad [26]$$

where Γ represents the gamma function. $\left|G*(\omega)\right|$ can then be computed for each MSD & time-scale point and used to compute the elastic and viscous modulus:

$$G'(\omega) = \left|G*(\omega)\right| \cos(\pi\alpha(\omega)/2)$$

$$G''(\omega) = \left|G*(\omega)\right| \sin(\pi\alpha(\omega)/2). \qquad [27]$$

2.3.2 Two-Point Particle Tracking Microrheology

While PTM has been shown to accurately measure the shear modulus in homogeneous systems, its validity in heterogeneous systems is disputed, especially when particles used are much smaller than the length scale of heterogeneity. To better understand why that is, it is best to visualize particles that have been embedded in a heterogeneous system such as mayonnaise. Although in bulk mayonnaise appears to be homogeneous, at smaller (micron) length scales the system is heterogeneous, consisting of regions, which vary in viscoelasticity (see Figure 2.6). Unlike homogeneous systems, the particle's motion will vary by location and will yield a large range of MSDs all scaling differently with different power-laws. For example, a particle constrained in a pore will probe only local mechanical properties characteristic of the pore alone.

More recently, Crocker et al., (2000) developed a method, which takes advantage of the "statistically cross-correlated Brownian motion of pairs of embedded particles", known as Two-Point particle tracking Microrheology (TPM). TPM aims to quantify the long range random fluctuations of the material by cross-correlating the displacement vector along a given direction of two particles embedded within the material. Since the strain field of a particle will entrain another particle at a distance d differently from other particles, the cross-correlation of particle-pairs will yield a measure of the strain field in the material (Valentine, 2003). In a homogeneous material, the cross-correlation will be proportional to an individual tracer's MSD and will decay as a/d, where a is the tracer's radius while d is the distance between a pair of cross-correlated particles. In heterogeneous system, the cross-correlation will not be proportional to a particle's individual MSD. In this case, one can obtain the bulk

mechanical properties by transforming the measured cross-correlation into an MSD (as will be shown below). The cross-correlation is a measure of what is known as the random fluctuation of the material as a whole (Levine *et al.,* 2000).

Figure 0.6: Particles (orange) constrained in various pores within a heterogeneous system. In cells, these pores can be made up of various bio-polymers which make up the cytoskeleton.

Obtaining the Two-Point MSD is a computationally intensive task requiring computing the cross-correlated motion of all tracer pairs within a given range of separations in a frame at various time-scales for all frames. A large amount of particles (a minimum equivalent of 100 particles per image over ~ 10000 images) are required to obtain valid measurements of the Two-Point MSD. For a good discussion on the statistical requirements to compute a Two-Point MSD, see Crocker *et al.,* (2000).

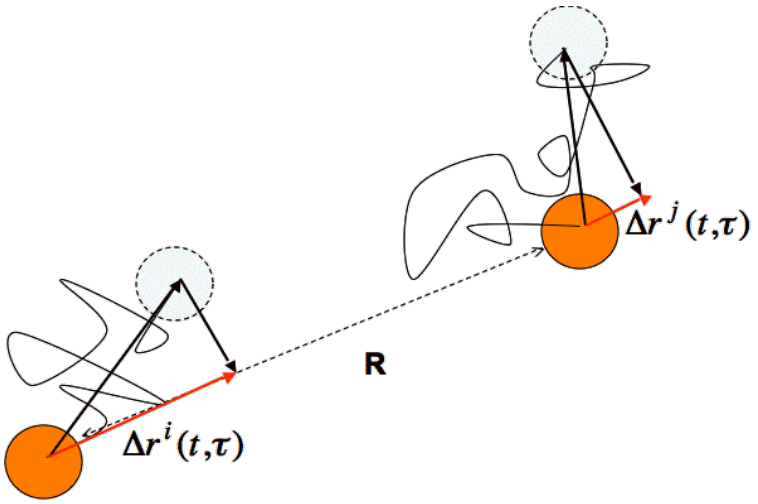

Figure 0.7: The orange particle is the original position and the broken line particle is the particle's location after a time step τ. By correlating the vector displacement along the direction of separation of two particles, a measure of the material's random fluctuation as a whole is obtained.

Computing the Two-Point MSD requires first obtaining the vector displacement of all tracers in an image for all time points *i* at various time scales τ (see Figure 2.7)

$$\Delta r_{\alpha}^{i}(t,\tau) = r_{\alpha}^{i}(t+\tau) - r_{\alpha}^{i}(t), \qquad [28]$$

where $r_{\alpha}^{i}(t)$ is the vector position of bead *i*, at time *t*. α represent a coordinates component of a given coordinate system. So if working in the cylindrical coordinate system, then α can represent the vector displacement in the direction of the particle-pair separation.

The ensemble averaged cross-correlation of particle-pair displacements can be computed by multiplying the vector displacement of particle *i* and particle *j*, which are separated by a given distance *d* for a lag time τ and averaged over all i ≠ j and time t.

$$D_{rr}(\boldsymbol{d},\tau) = \left\langle \Delta r_r^i(t,\tau)\Delta r_r^j(t,\tau)\delta[\boldsymbol{d} - R^{ij}(t)] \right\rangle_{i\neq j,t}, \qquad [29]$$

Here, R^{ij} is the separation between tracer *i* and *j*, a is the tracer radius and δ represents the Dirac (delta) function**.** It is then important to verify that D_{rr} scales as *1/d*, which indicates that the medium can be treated as an incompressible continuum system at the length scales *d*. The Two-Point MSD is obtained from D_{rr} as follows:

$$\left\langle \Delta r^2(\tau) \right\rangle_D = \frac{2d}{a} D_{rr}(d,\tau), \qquad [30]$$

TPM is not affected by surface chemistry interaction of the tracer and material and is able to measure bulk mechanical properties in heterogeneous materials. Its greatest disadvantage is the large number of particles and long videos required to make statistically significant measurements. Crocker et al. (2007a) report that a minimum equivalent of 10,000 images, each containing ~100 tracers yields satisfactory results. The technique is also highly sensitive to noise caused by large vibrations or drift within the sample. In cells, active intracellular processes tend to cause directed motion of processes masking the tracer's Brownian motion. Therefore, it is advisable to apply the method to cells that have been depleted of ATP.

Chapter 3

Methodology

3.1 Overview of Experiments

The first three sections of this chapter describe the experimental set up, sample preparation and experimental procedures of PTM experiments proposed in the first chapter of this thesis. These include PTM validation experiments with glycerol and guar, and PTM experiments that aim to measure the mechanical properties of cells undergoing chemotherapy. Glycerol, a purely viscous material, was used to a) measure the MSD at three bead concentrations, b) validate PTM's ability to detect viscosity changes, and c) help develop an understanding of the limitations on quantifying mechanical properties using PTM. Guar was used to validate PTM for measuring viscoelastic properties. The experiments are set up to a) verify that PTM can measure the elastic component when it is present, b) that the elasticity measurement is proportional to increasing guar concentration, and c) the ability of PTM and TPM to quantify the bulk rheology of the material. Cisplatin treated PC3 cells are then used to study the change in mechanical properties for 12 hours using PTM. The final section of the chapter illustrates how the mechanical properties of materials are obtained from short movies of tracers collected during the experiments.

3.2 Experimental Setup

Intracellular Particle Tracking Microrheology (PTM) experiments require that tracers be present within a material of interest. While some PTM experiments utilize endogenous tracers such as lipid granules (Lau, Hoffman, Davies, Crocker, & Lubensky, 2003), others introduce particles into the cell by endocytosis or microinjection (Weihs, Mason, & Teitell, 2006). It is important that in PTM, particles are only caused to move by the thermal energy of the system (Brownian motion) and that no active forces direct the motion of these particles. Endogenous tracers and tracers introduced to the cell via endocytosis are more susceptible to active mechanical forces which take place within a cell (Weihs, Mason, & Teitell, 2006), while Valentine et al. (2004) showed that carbohydroxilated modified particles microinjected into the cell can help avert protein attachment, and therefore avoid active forces directing the movement of particles.

A Xenoworks microinjection system along with a micropipette puller (Sutter, Inc., Los Angeles, CA) was used for microinjection of cells. The system allows for the use of custom tailored micropipettes for microinjecting fluids or micro-particles as well as for the application of pressure (or suction) gradients along the surface of the cell. Pressure ranges of -350 to +350 hPa at 7 hPa steps are available for injection and suction, while a higher pressure used to clear the pipettes can go up to 5600 hPa. Micropipettes are controlled by a joystick which allows for high-precision movement (~100 μm displacement of pipette for a full swing of the joystick) along the *x*, *y* and *z* axes. Carbohydroxilated fluorescent particles 0.2 μm in diameter were (Invitrogen™, Carlsbad, CA) dialyzed in DPBS as described in Kole et al. (2004). An Olympus IX71 inverted microscope (Olympus, Inc. Markham,

Ontario), with objective lenses of 10x, 40x, and 100x magnification, and a lever which, when pulled, multiplies the objective lens' magnification by 1.6x, was connected to the microinjection system. Huffman Modulation Contrast (HMC) is available with our system for the 10x and 40x magnification. HMC is designed to increase visibility and contrast in unstained and living material by detecting optical gradients (or slopes) and converting them into variations of light intensity [2]. As the particle probe size is limited by the wavelength of light in standard video light microscopy to ~0.4μm, a fluorescence illumination system was purchased (EXFO Inc., Quebec, QC) and was connected to the system. This permitted the use of particles as small as 0.2 μm.

A Retiga EXi CCD camera (QImaging Inc., Surrey, BC) was mounted on the microscope and connected to a local personal computer via firewire. Streampix software (Norpix Inc., Montreal, QC) was used with the camera to capture videos that were converted into TIFF frames. At full resolution, videos could only be captured at 12 frames-per-second (fps). Reducing the exposure time, the frame size, and averaging grouped pixels[3] can increase the capture rate up to 110 fps. In other words, compromising spatial resolution helps improve on temporal resolution. These parameters are set differently for each experiment while ensuring that a minimum of ~ 4 pixels per tracer as required for tracking was used. Five movies or more were collected per sample at different locations in the sample due to statistical requirements (enough frames and particles per frames). Images captured without grouping pixels at 40X and 100X magnification had square pixels of 0.1613 μm and 0.0645 μm, respectively. This was verified by using a calibration cover glass.

[2] http://www.olympusmicro.com/primer/techniques/hoffman.html

A micro-perfusion and temperature control system (Bioptech Inc., Butler, PA), which mounted to the microscope, was used to maintain cells in a suitable environment for live imaging under bright field and HMC. Fluctuations in the focal plane were observed when the system was used with the oil based 100X magnification due to the objective acting as a heat sink when the oil came in contact with the dish. Because of this, the temperature control and micro-perfusion system were not used for PTM experiments; it was only used to capture HMC images of treated cells to confirm that structural changes associated with apoptosis are observed.

3.3 Sample Preparation

Glycerol (Medisca Inc., Plattsburgh, NY) was mixed with water at four different weight-by-weight concentrations: 30%, 50%, 70% and 90%. Polystyrene particles, 0.2 μm in diameter, were added at three concentrations: (A) 1.52 x 10^9 particles/ml (B) 13.6 x 10^9 particles/ml and (C) 28.8 x 10^9 particles/ml, and mixed using a magnetic spinner for 20 minutes. A sample of 100 μl from each of the 12 solutions prepared was deposited into a PC20 chamber (Grace Bio-Labs Inc., Bend, OR) and sealed using 0.17 mm thick cover glass purchased from Fisher (Fisher Scientific Company, Ottawa, ON).

Guar (Sigma-Aldrich Inc., Oakville, ON) was purified as explained by Pai *et al.* (2002). Purified guar was left to dry into powder form, and then mixed with different concentrations of water to obtain three weight-by-weight guar solutions of 0.25, 0.5 and 0.8%. 0.2 μm polystyrene particles were mixed with the three solutions at a concentration of

[3] Also refered to as binning pixels by QImaging Inc.

13.6 x 10^9 particles/ml (this value is chosen based on validations done with glycerol, see results and discussion). The solutions were then centrifuged at 40,000 rpm for 20 minutes to eliminate air bubbles. A sample of 100 μl from each of the three solutions prepared was deposited into the PC20 chambers and sealed using thin 0.17 mm cover glass.

PC3 (prostate cancer) cells were cultivated for two weeks in F12K media containing antibiotics, HEPES and Felum Bovine Serum (FBS) prior to intracellular particle tracking microrheology experiments. Cells were trypsonized and split into four Delta-T dishes (Bioptech Inc., Butler, PA). Cells were then serum starved 24 hours after trypsonization and incubated. After incubating for 24 hours, three out of four dishes were taken out of the incubator for microinjection with beads. As many cells as possible were microinjected within an area marked by a circle on the dish's bottom glass (see Appendix A for microinjection procedure). This is done within 25 minutes in order to avoid cell contamination outside of the incubator. In this time, typically 30-40 cells were injected. Cells were then washed with PBS three times and new media was added to the dish. Microinjected cells were left for 24 hours in the incubator to allow particles to diffuse throughout the cells. It should be noted that cell survival is strongly dependent on the microinjection technique and manipulation of the pipettes as discussed in (Panorchan et al., 2007; Viigipuu et al., 2004). The fourth dish was used to image the changes in apoptotic cells at different time points using light microscopy.

3.4 Experimental Procedure

3.4.1 Glycerol and Guar

Individual PC20 chambers loaded with sample (guar or glycerol) were placed under the microscope and imaged at a magnification of 100x. The focal plain is set a few micrometers above the bottom glass wall of the chamber to avoid boundary effects. Particles were excited with fluorescent light for imaging and five videos, each containing 5000 frames, were captured at different locations in the sample chamber. Room temperature was measured to be approximately 25°C at the time of glycerol experiments and 23°C during guar experiments. All videos were captured at 40 fps (highest frame rate possible by optimizing camera parameters discussed in section 3.2), with an exposure time of 20 ms and pixel binning for a final pixel size of 0.12 μm.

The bulk loss and storage modulus of 0.25% guar was also measured using a C-VOR 150 Bohlin rheometer (Malvern Inc., Worcestershire, UK) for comparison. Samples were probed at 25°C with a strain amplitude of 0.1% (based on a strain test performed before the experiments) when using the rheometer.

3.4.2 Cells

Cisplatin, a chemotherapeutic agent used for chemotherapy, was introduced at a concentration of 0.1 mg/ml into all four dishes 3 hours before the first videos were captured. The dish containing the most cells surviving the microinjection process was chosen for the microrheology experiments. The chosen cell dish was kept in the incubator and taken out for 25 minutes only when videos are to be captured. Approximately 12 videos, each 1000

frames long, were captured at the 100X magnification at four time points. Videos were kept short to avoid photobleaching of particles. Cells were selected in the dish within the marked microinjected region. Videos were taken at the 3, 6, 9 and 12-hour points after exposure to cisplatin. The number of videos captured was dependent on the number of cells available that survived microinjection. At later treatment time points, videos captured focused on cells that expressed signs of apoptosis such as morphological change, blebbing[4] or shrinkage. The exposure time was set between 10-20 ms, and image pixels were grouped and averaged[5], yielding a final pixel size of 0.12 μm. Videos of the fluorescent particles were captured at 25 fps. The maximum video capture frame rate is determined by parameters discussed in section 3.2 of this chapter. These parameters were set using trial and error as to ensure that all particles present within a cell are clearly visible in the video.

The fourth dish (containing non-microinjected cells) was used to image cells for a continuous 12-hour period by maintaining it under the microscope using the micro-perfusion pump and temperature control system. These images were not used for the PTM experiments, but are simply used to visualize characteristics of apoptosis. Images are captured at 1 frame/10 minutes at the 40X magnification.

3.5 Data Analysis

Beads were individually tracked using specially written MATLAB routines. These routines were originally written in IDL by Crocker et al. (1996) and ported to MATLAB code by

[4] A **bleb** is an irregular bulge in the plasma membrane. Blebbing is the term used to describe the formation of blebs.

[5] Also refered to as pixel binning by QImaging Inc.

Daniel Blair and Eric Dufresne[6]. Tracking particles can be broken down into four stages: 1) correcting image imperfections and filtering noise, 2) accurately locating particle positions for each frame, 3) filtering unwanted track or particles, and 4) linking positions into tracks for a collection of frames.

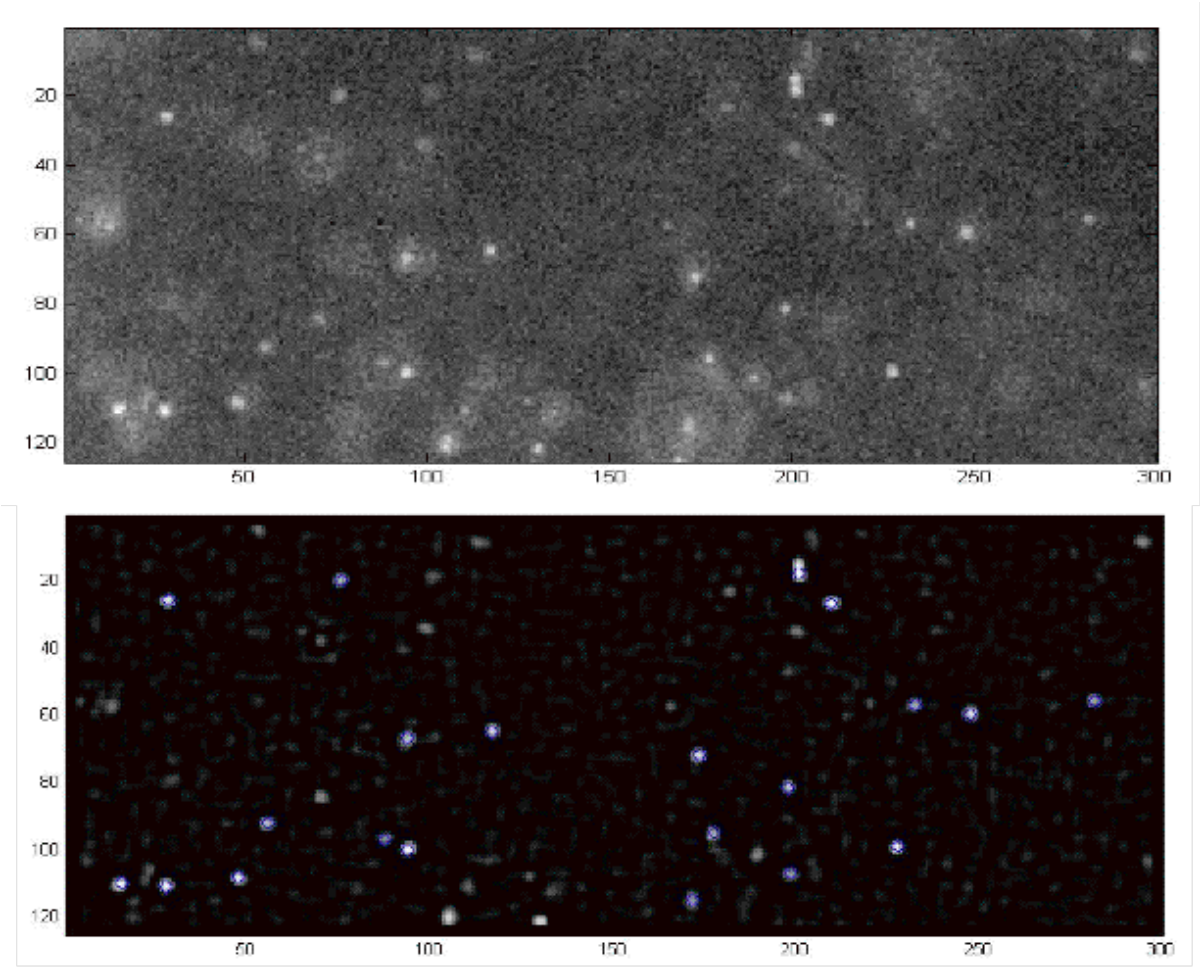

Figure 0.1: The top picture shows a captured image of fluorescent particles before tracking and applying the bandpass filter. The bottom picture shows the same image after filtering and finding particles to be tracked. The blue circles indicate particles to be tracked.

[6] http://physics.georgetown.edu/matlab/

Correcting image imperfections is done using a band-pass filter included with the routines mentioned above. Essentially, the filter reduces both low spatial frequency (shading) and high spatial frequency (snow) contributions to the image. The program uses a bandpass filter to remove the random digitization noise and background respectively (Crocker & Grier, 1996). The filter yields a better signal-to-noise ratio and improves the image for tracking as observed in Figure 3.1. Filtered images will effectively consist of bright spots on a dark background, which will aid the following algorithms to determine the location of particles.

Next, a routine is used to find the brightest pixels in the image and the brightness distribution (from other pixels) surrounding that pixel. These peaks label the location of potential particles to be tracked. The particle location is assumed to be the brightness-weighted centroid. These routines have been shown to accurately determine the centre of a spot to sub-pixel accuracy. The program requires the user to specify the brightness threshold of particles to be used. The algorithm is also able to compute other properties of each particle including the total image brightness as well as the average size of each blob, otherwise known as the radius of gyration.

Computer routines were created as well to avoid particles that are clumped together or near each other (less than the particles diameter) since these can be mistaken for a single particle. The routines use the radius of gyration to exclude any particles that were larger than 12 pixels (~ 1μm). Although particles are 0.2μm in physical size, they appear to be larger (0.4-0.6μm) under the microscope due to fluorescence illumination, hence why the above-mentioned threshold is set at 1μm (approximately double the diameter of the particles when fluorescing). Since the radius of gyration is an approximate measure of the radius of a

particle, it makes a suitable parameter to be used for this sort of filtering. More precautions were taken in cell experiments, where each particle found by the algorithm is examined individually to ensure that it is indeed within the cell and not clumped with other particles.

The final step to tracking involves linking all found particles temporally in the sequence of images. Particle locations were formed into tracks based on a frame-to-frame maximum displacement threshold (frame-to-frame proximity) that was operator selected. The routine requires that the user inputs a maximum distance traveled in one time step of the video. This threshold should be sufficiently larger than the maximum distance traveled but not larger than the minimum distance between particles. Generally from observations, for 0.2 μm particles, it can be expected that in a 30% weight-by-weight concentration solution of glycerol, particles will not move more than ~8 pixels, on average, in the smallest time step. From our sample preparations, the highest concentration of particles usually had a particle-to-particle separation of 15 pixels or more. Camera noise can also cause spurious particles to be tracked. These are generally short tracks, which can be eliminated by setting a minimum track length in the track linking routine.

All further analysis was done using code provided by Dr. Maria Kilfoil at McGill University, for the exception of minor code written by me to aid in my analysis. Dr. Kilfoil's code computes the PTM and TPM MSD as well as the complex shear modulus, and is a direct translation to MATLAB from IDL code originally written by Crocker et al. (2000). Before computing the MSD and the mechanical properties, a de-drifting routine was used to eliminate obvious drift observed in tracks[7]. The MSD was then computed from the de-drifted

[7]See: http://www.physics.emory.edu/faculty/weeks/idl/motion.html.

tracks obtained by the tracking program. The MSD was determined using the mean of all displacements at a given lag-time, using all frames and particles:

$$\left\langle \Delta r^2(\tau) \right\rangle = \left\langle (r(t+\tau) - r(t))^2 \right\rangle, \qquad [40]$$

where $r(t)$ is a single position at a specific time point in the video, τ represents the time scale or the lag-time at which the MSD is being computed and $\langle ... \rangle$ now indicates time and ensemble (over all particles) average.

The TPM MSD was also computed from the guar and glycerol experiments. Four parameters were needed by the routine as input: a minimum and a maximum distance for correlation, the number of bins in which to store correlations at different separations and a maximum time-scale to correlate the particles over. Generally speaking, the minimum correlation distance should be set to a value that is much larger than the length-scale of heterogeneity. It is also important to keep in mind that the images of closely spaced particles can overlap, adding a spurious cross-correlation to their motion and confounding the TPM measurements (Crocker *et al.* 1996). Lau *et al.* (2003) found that using a minimum correlation distance of 2μm generally works well. The maximum separation is generally defined by the finite size of the sample, i.e. diameter of a cell, but can be set to any value that is smaller than the maximum size of the sample. The number of bins that the spatial correlation data are stored in is usually determined & optimized by trial and error. A greater number of bins give more points to evaluate the spatial behavior, but also decrease the statistical power in each

point. Finally, the maximum lag-time over which particles will be correlated should be set to a value less than the length of time a particle remains in the focal plain. This is to ensure that enough particles are tracked at higher lag-times to meet statistical requirements. This value is set to a maximum of 2 seconds. The TPM algorithm yields a MSD representative of the random system fluctuation within a range of time scales. MSDs are plotted on log-log plots against time-scales (lag-time). The root mean square (noise floor) of the system was estimated by immobilizing particles and tracking them as described in Kole et al. (2004). At 100X magnification with binned pixels, the noise floor was in the ~ 10^{-6} um^2 range, which is lower than MSD measurements from any sample.

The complex shear modulus was then extracted from the MSD as described in the theory section of this text. Mason (2000) states that computing the shear modulus with an algebraic method will always introduce artifacts known as truncation errors. These errors are usually present at the frequency edges of the shear modulus. The slightest curvature or ripple in the MSD will cause such artifacts when the shear modulus is being computed. To avoid these, the MSD is truncated to ignore points where no trend is observed.

Chapter 4

Results & Discussion

4.1 Results

4.1.1 Glycerol

Figure 4.1 shows images containing: (A) 1.52 x 10^9 particles/ml (B) 13.6 x 10^9 particles/ml and (C) 28.8 x 10^9 particles/ml.

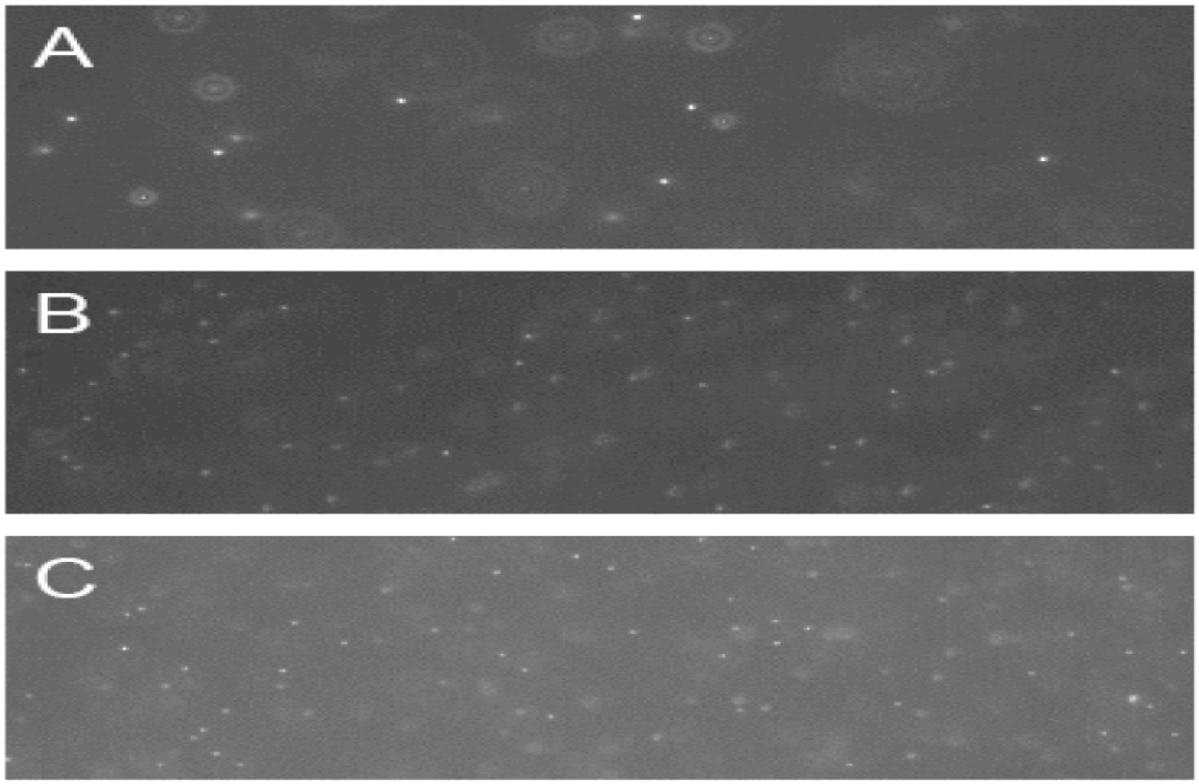

Figure 0.1: Images of three different particle concentrations: (A) 1.52 x 10^9 particles/ml (B) 13.6 x 10^9 particles/ml and (C) 28.8 x 10^9 particles/ml.

Five 5000-frame (~2 minutes at 40 FPS) videos are captured and used to compute the MSD at all time-scales up to 2 seconds in all 12 solutions. An ensemble-average of individual tracer MSD for each of the solution is then computed and plotted on a log-log graph (Figure 4.2). Figure 4.3 and 4.4 show the MSD of each individual particle in all four glycerol concentrations for the highest bead concentration.

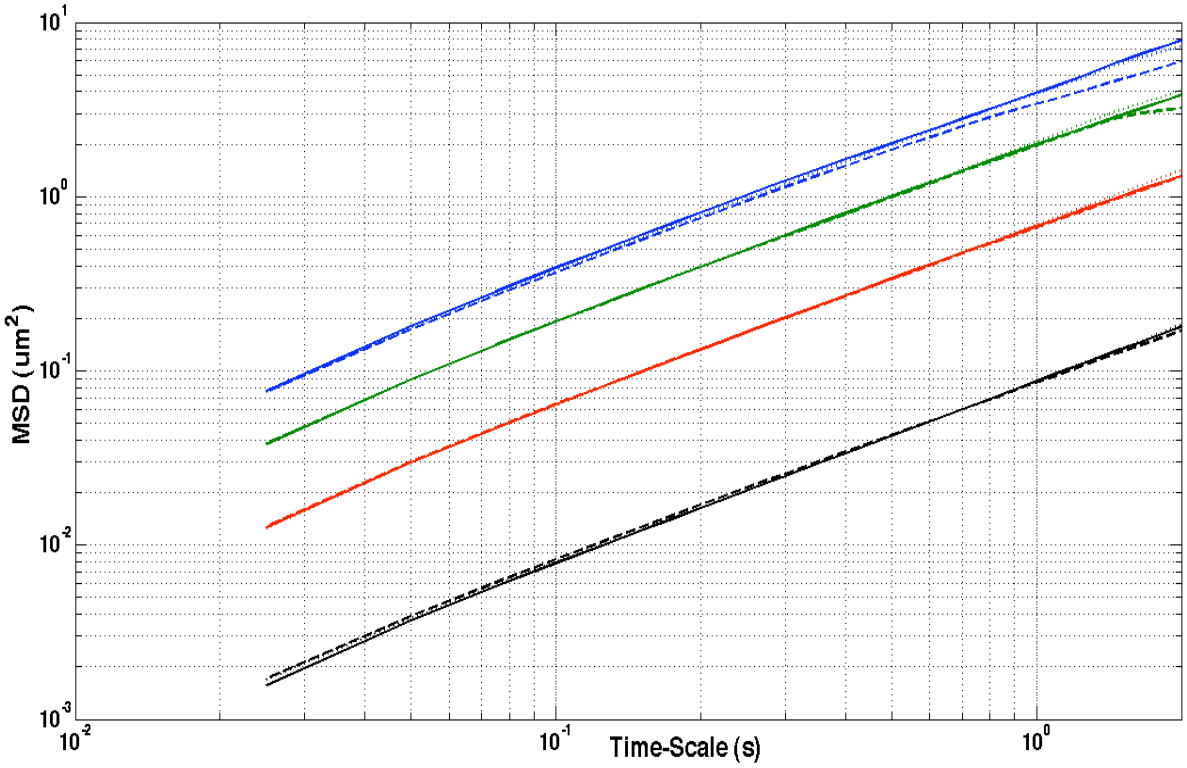

Figure 0.2: MSD plots for all 3 particle concentrations: (• • • • •) 1.52 x 10^9 particles/ml (- - - -) 13.6 x 10^9 particles/ml and (———) 28.8 x 10^9 particles/ml, and glycerol concentrations: a) 30% (blue) b)50% (green) c)70% (red) d)90% (black).

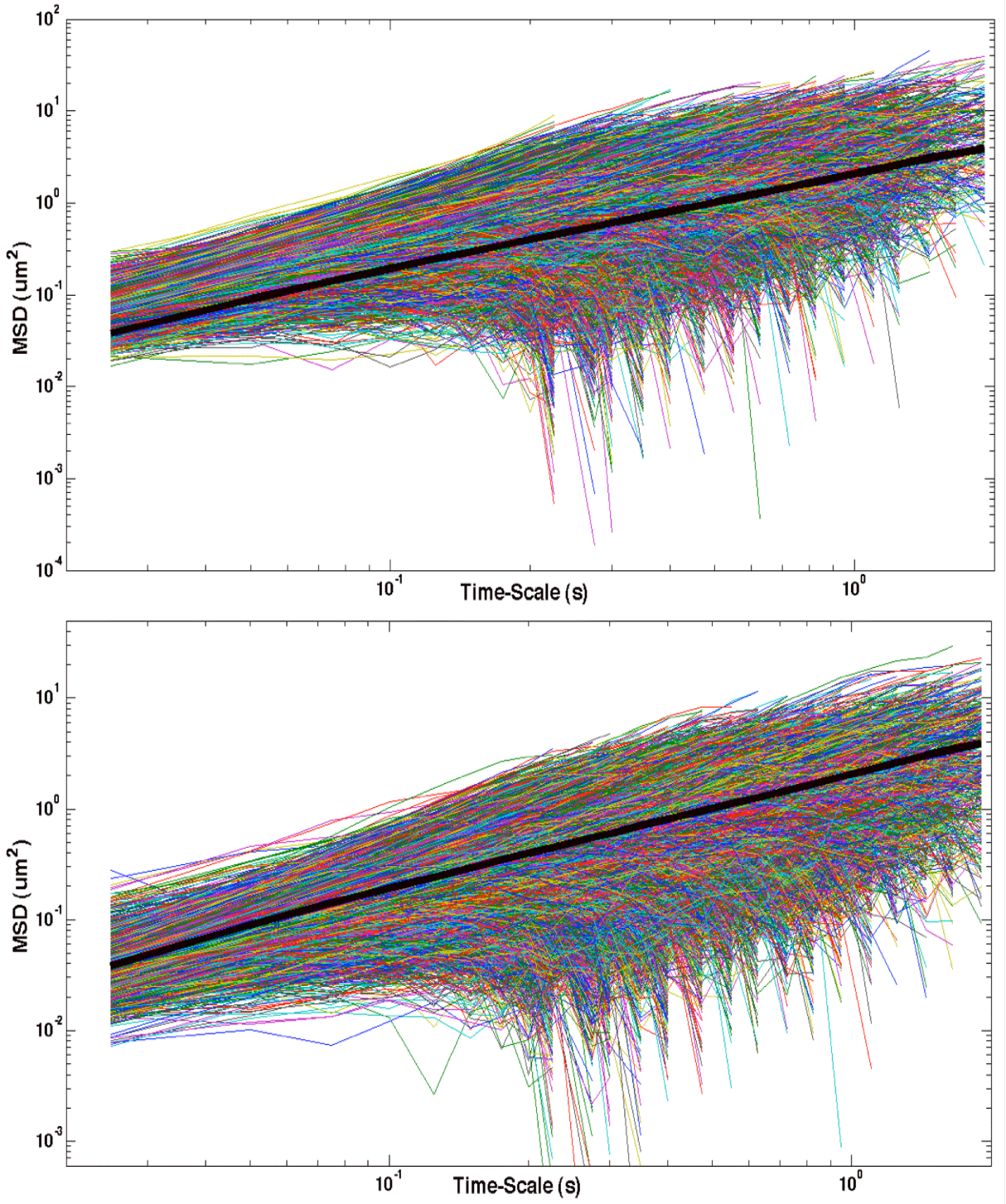

Figure 0.3: Individual tracks (>1000) for 30%(top) and 50%(bottom) glycerol. The thick middle line is the ensemble average of all MSD present on the plot.

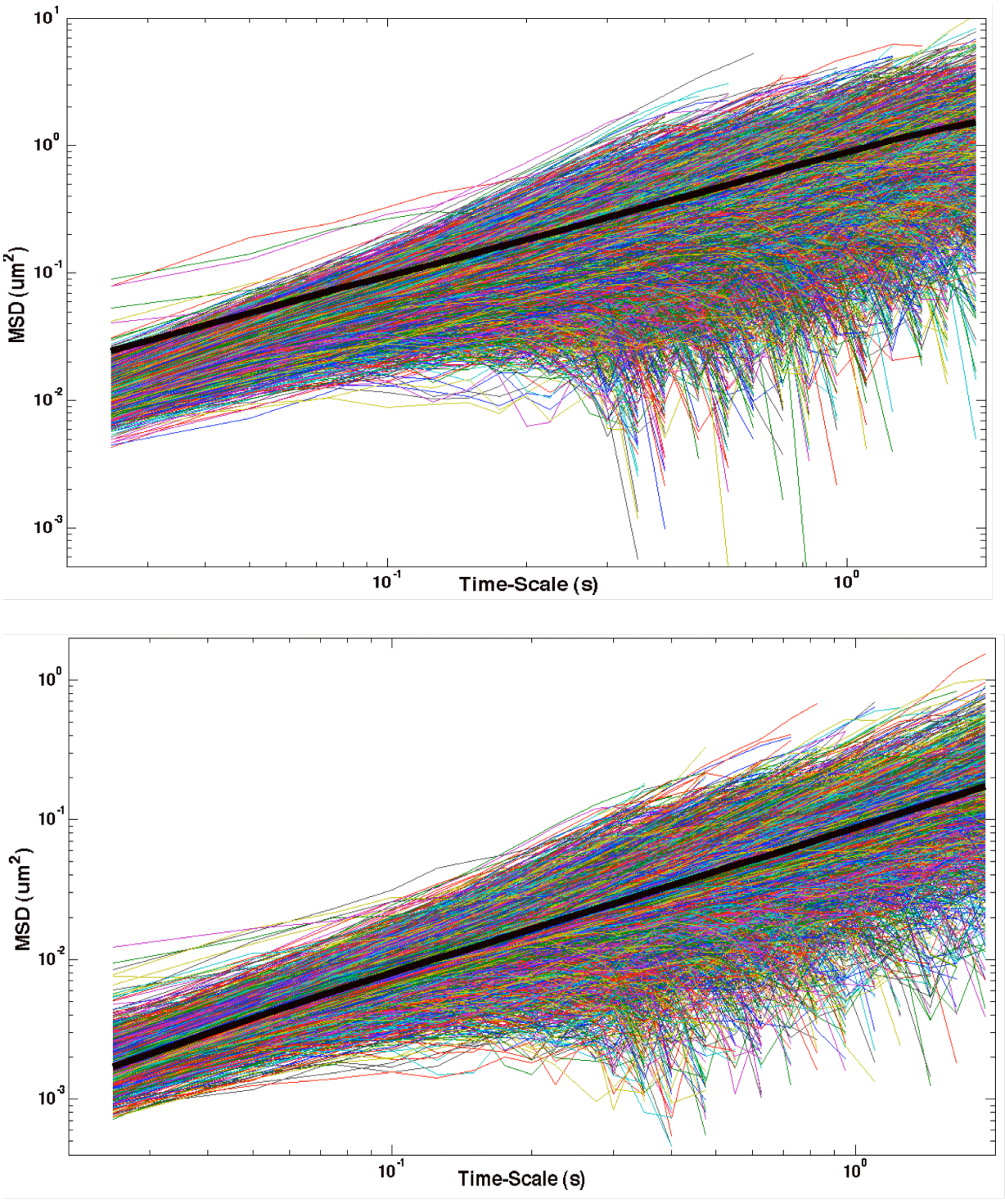

Figure 0.4: Individual tracks (>1000) for 70%(top) and 90%(bottom) glycerol. The thick middle line is the ensemble average of all MSD present on the plot.

Concentration	Rheometer*	PTM	Deviation Error
30 %	2.141 cP	2.2 cP	4 %
50 %	4.642 cP	4.2 cP	9 %
70 %	16.62 cP	13 cP	22 %
90 %	132 cP	103.2 cP	22 %

Table 1: Viscosity obtained by both PTM and a rheometer[8]. All experiments are done at room temperature.

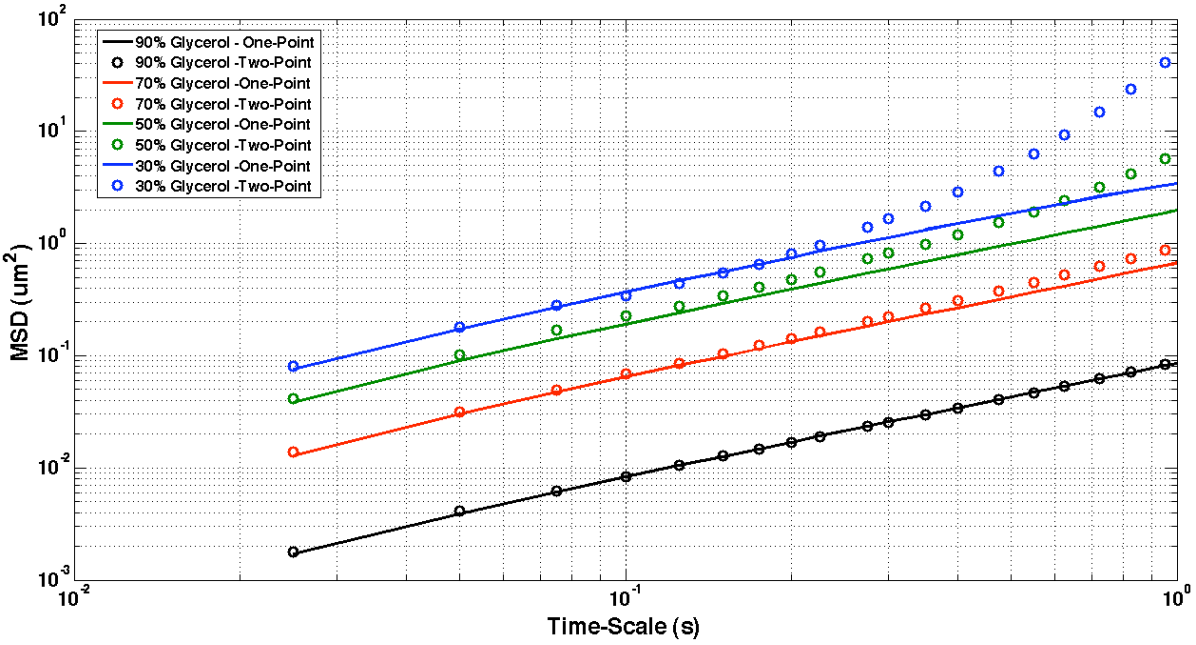

Figure 0.5: PTM (solid lines) and TPM (circles) MSD for all four glycerol concentrations with a bead concentration of 28.8 x 10^9 particles/ml.

As no significant variation is observed in the MSD of the three bead concentrations, the highest bead concentration is then used to compute the complex shear modulus of all four glycerol concentrations. No elastic component was measured (α=1). The frequency

[8] Rheometer viscosities obtained from http://www.dow.com/glycerine/resources/table18.htm

dependent viscous modulus is converted to a frequency independent viscosity measurement. Table 1 compares the viscosity measurements to previously published rheometer measurements of the same four concentrations. Tracks from all four glycerol concentrations (for the highest bead concentration) are used to compute the TPM MSD of the data and plotted in Figure 4.5.

4.1.2 Guar

After tracking particles and computing the average MSD for all tracks in each of the three guar samples (Figure 4.6), the complex shear modulus is computed and plotted against the frequency in rad/s on a log-log graph (Figure 4.8). Figure 4.7 shows the MSD of each individual particle in the 0.25% solution.

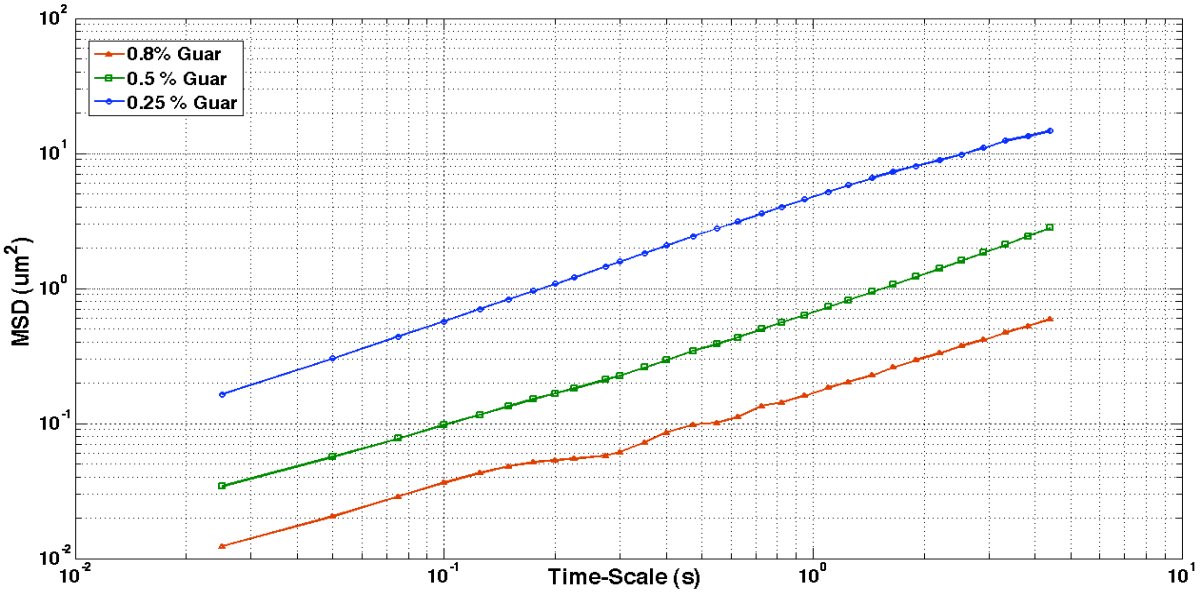

Figure 0.6: MSD for three different Guar concentrations. These MSD were used to compute the complex shear modulus presented below.

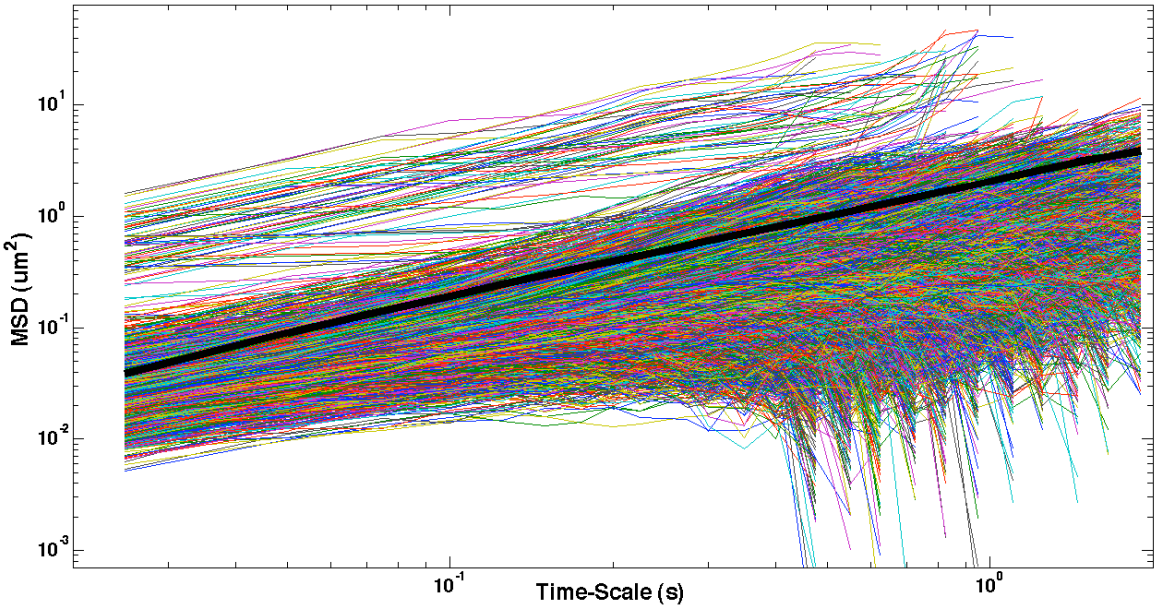

Figure 0.7: Individual tracks (>1000) for 0.25% guar. The thick middle line is the ensemble average of all MSD present on the plot.

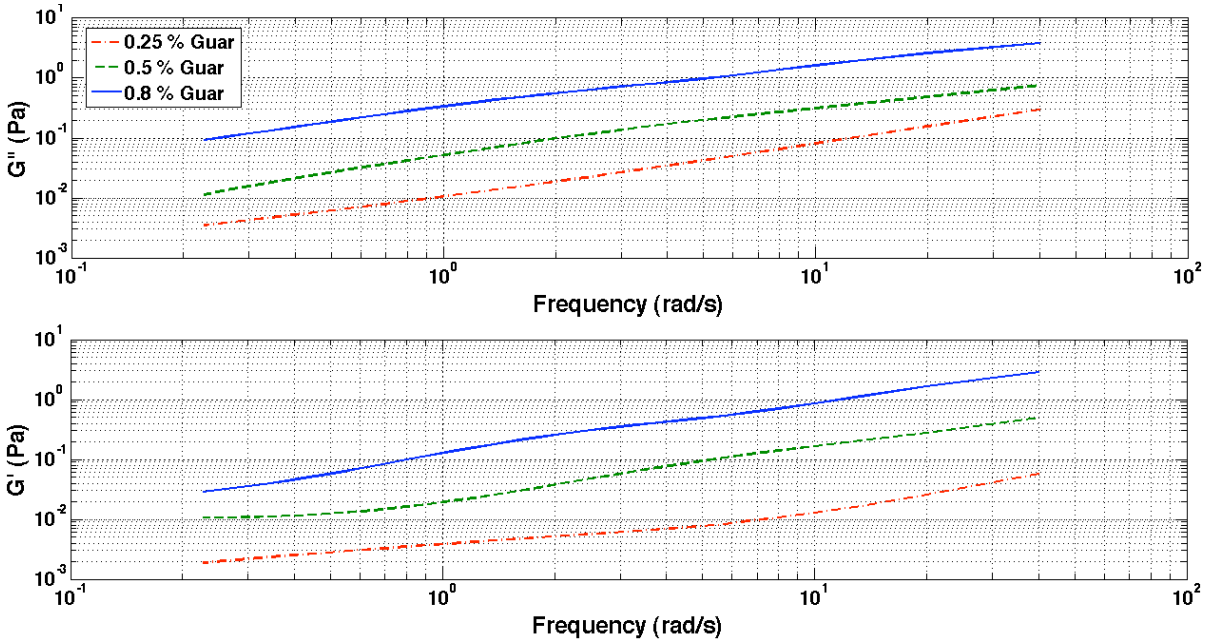

Figure 0.8: Viscous and elastic modulus of three guar concentrations. The top graph represents the viscous modulus and the bottom graph represents the elastic modulus.

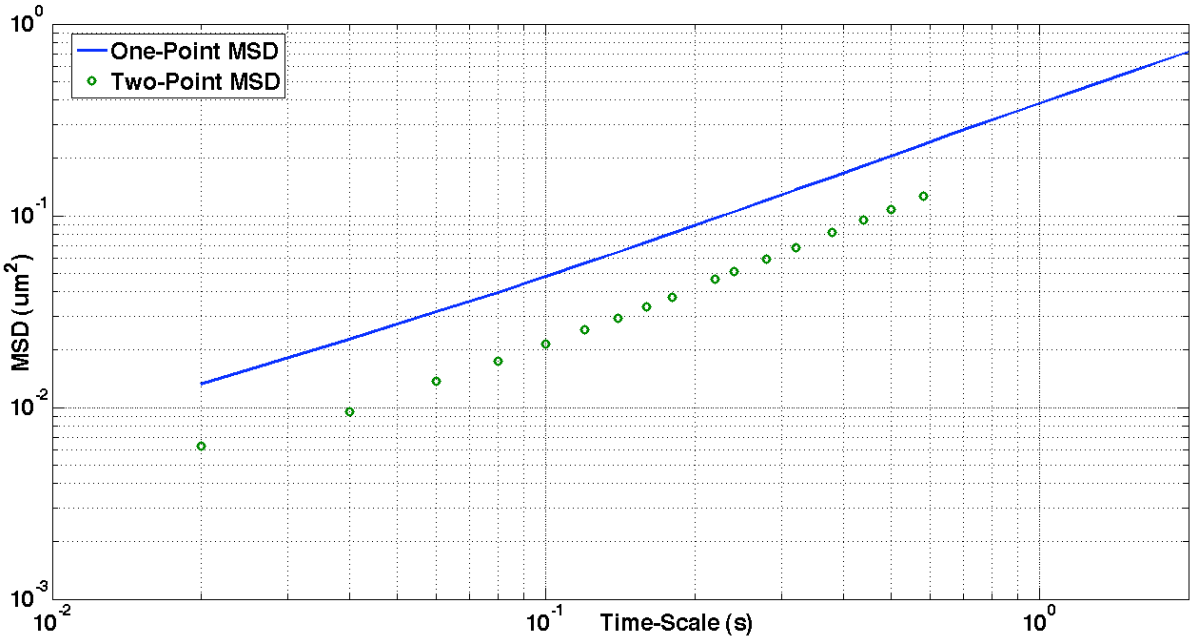

Figure 0.9: MSD for TPM (circles) and PTM (solid line).

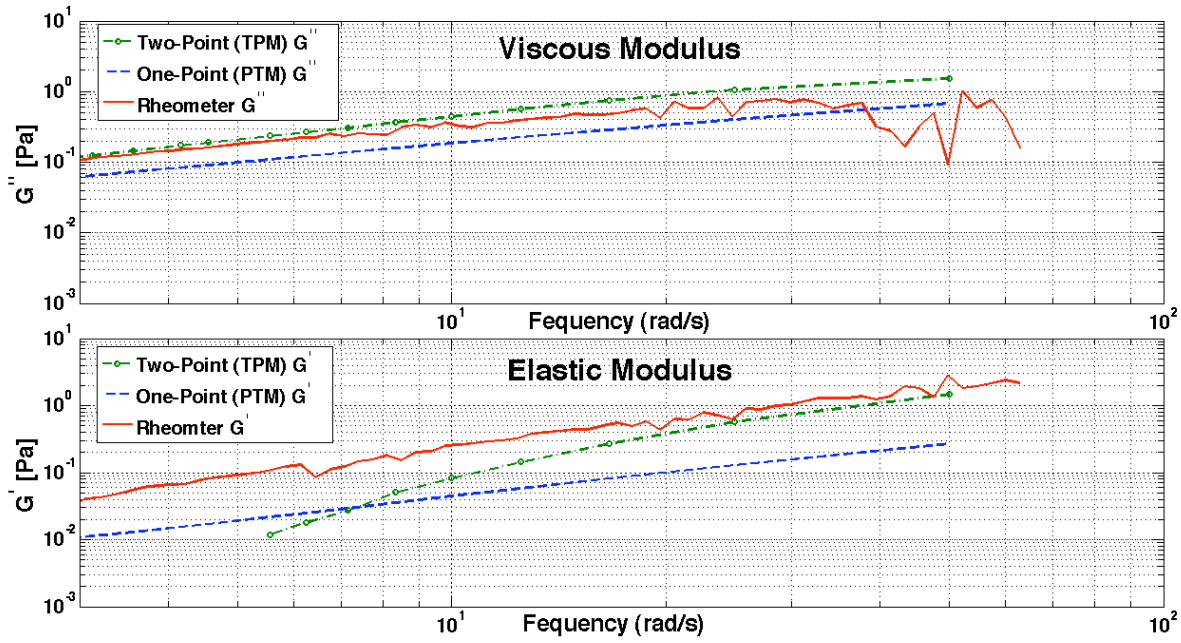

Figure 0.10: Comparison of three methods of obtaining the complex shear modulus: Rheometer (solid line), PTM (dashed line) and TPM (line with circles).

The TPM MSD for the 0.25% guar concentration is then determined. It is shown in Figure 4.9. Both MSDs are then used to compute the elastic and viscous modulus. The moduli are plotted on log-log graph along with the bulk elastic and viscous modulus obtained from the rheometer measurements (Figure 4.10).

4.1.3 Cells

Figure 4.11 shows the effects of serum starved cells exposed to cisplatin over four time points (3, 6, 9, 12 hours). Images are taken at 40x magnification over 12 hours.

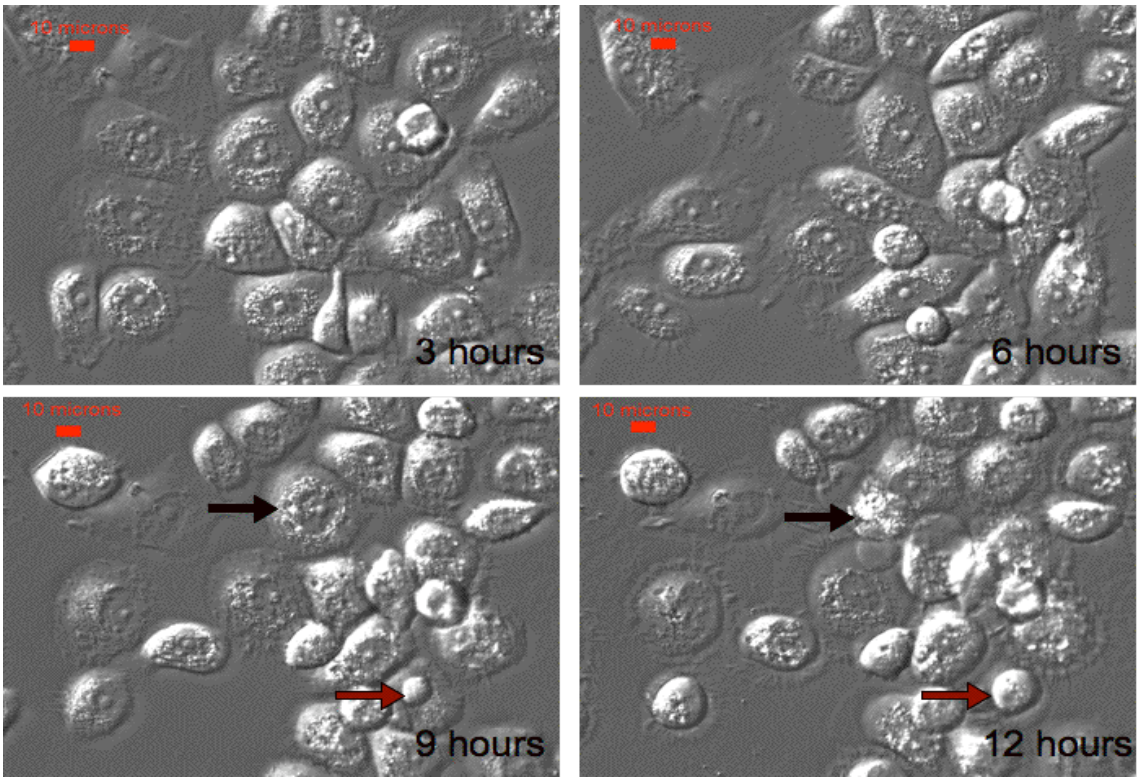

Figure 0.11: Effects of cisplatin on PC3 cells at four time points after exposure. At 3 and 6 hours, cells appear viable. At 9 hours, some cells start to detach off the glass dish and show morphological changes while at 12 hours, some cells start to show clear characteristics of apoptosis. The arrows point to cells which undergo significant change from the 9 to 12 hour point. The black arrow in the 12 hours image points to a cell showing blebbing while the red arrow points to a cell undergoing morphological changes and shrinkage.

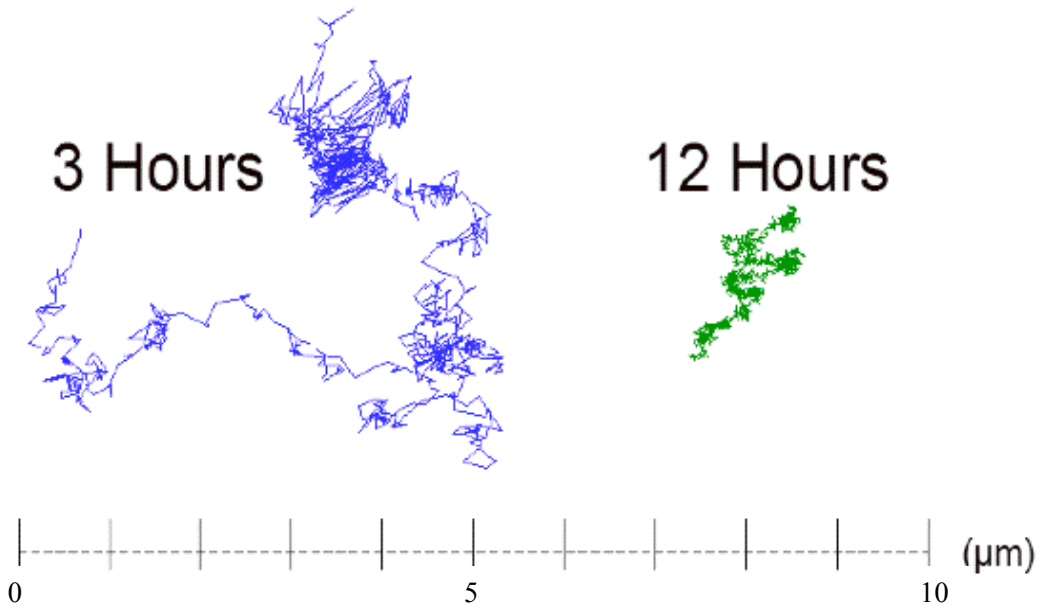

Figure 0.12: 40 second tracks of two randomly chosen particles at 3 hours and 12 hours. Particles are 0.2um in diameter and injected into cells 24 hours before exposure to cisplatin.

For PTM experiments, cells are kept in incubator during experiment and taken out for 25 minutes every 3 hours for imaging. Microinjected cells are picked randomly within the area of injection at the 3 and 6-hour point and imaged. At the 9 and 12-hour points, microinjected cells are imaged if signs of apoptosis (mostly morphology change, blebbing, nuclear fragmentation, etc.) are observed. After imaging, particles are tracked using MATLAB tracking software and the MSD was computed and plotted in Figure 4.13. Figures 4.14 and 4.15 show the MSD of each individual particle tracked at all time points.

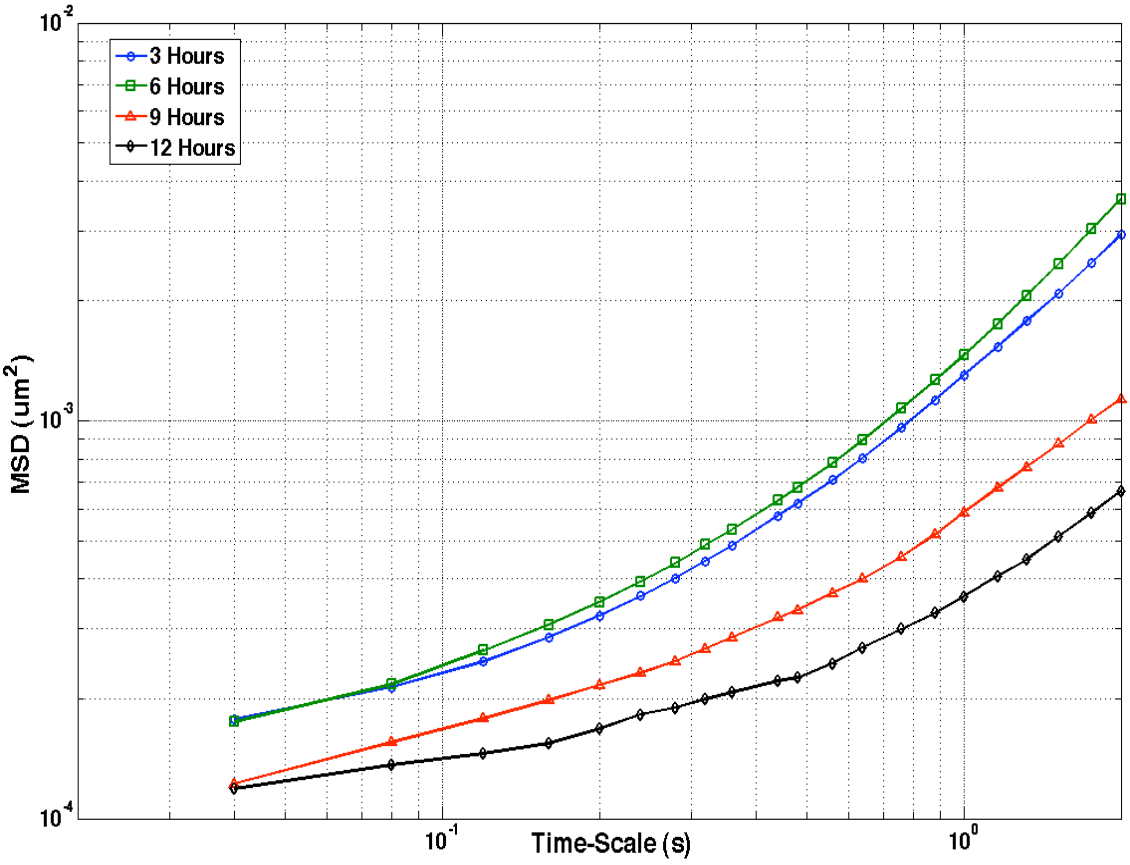

Figure 0.13: Average MSD of 0.2 um particles (~20 particles per time point) microinjected into cisplatin treated PC3 cells. The 3 and 6 hour points show no significant change in the MSD, while the 9 and 12 hour points seem to show a significant change both in the magnitude and the slope of the MSD. The reduction in the magnitude and slope of the MSD both indicate stiffening of the environment surrounding the particles.

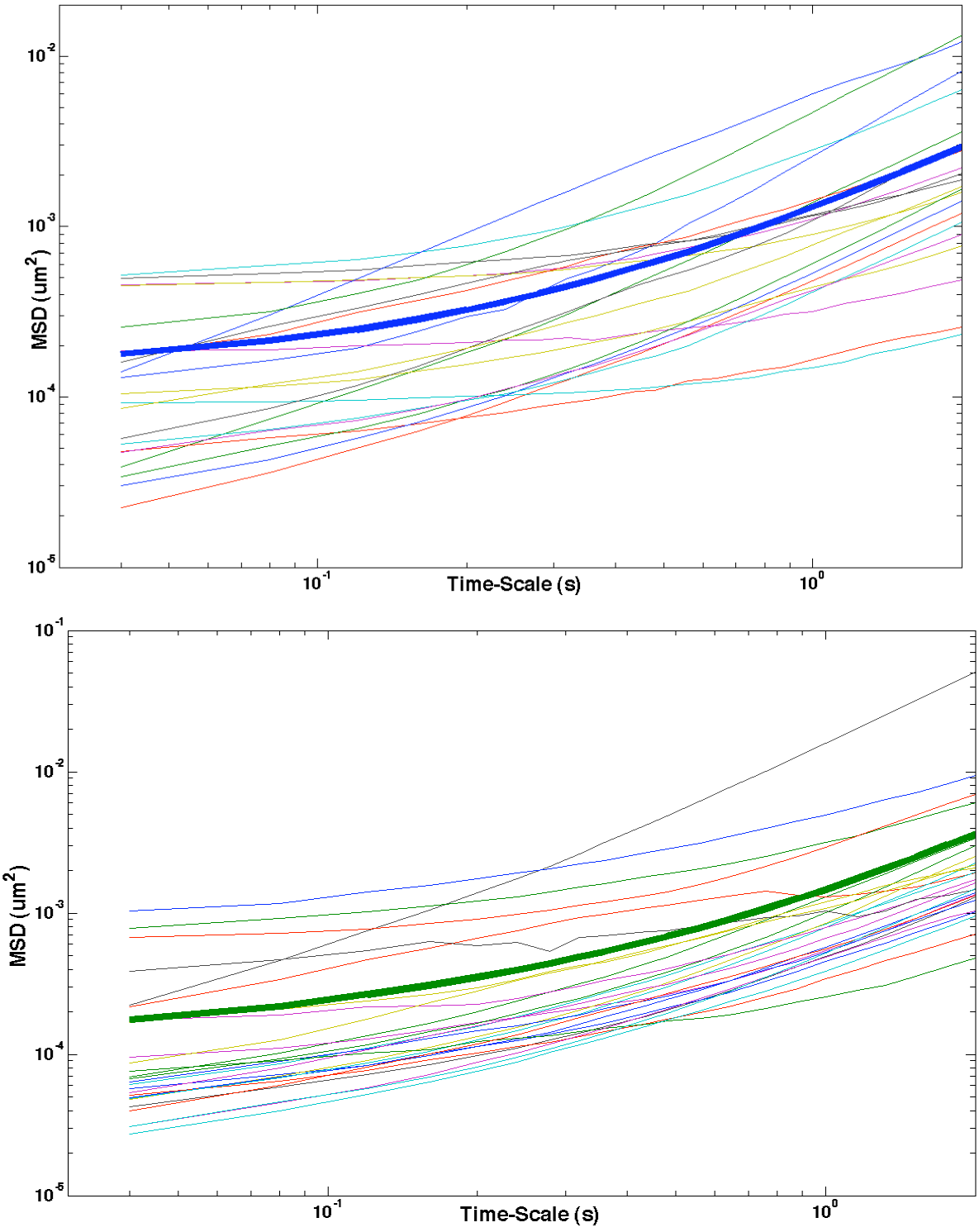

Figure 0.14: Individual MSD for particles tracked in cells at 3 hours (top) and 6 hours (bottom). The thick solid line represents the ensemble average of all MSDs.

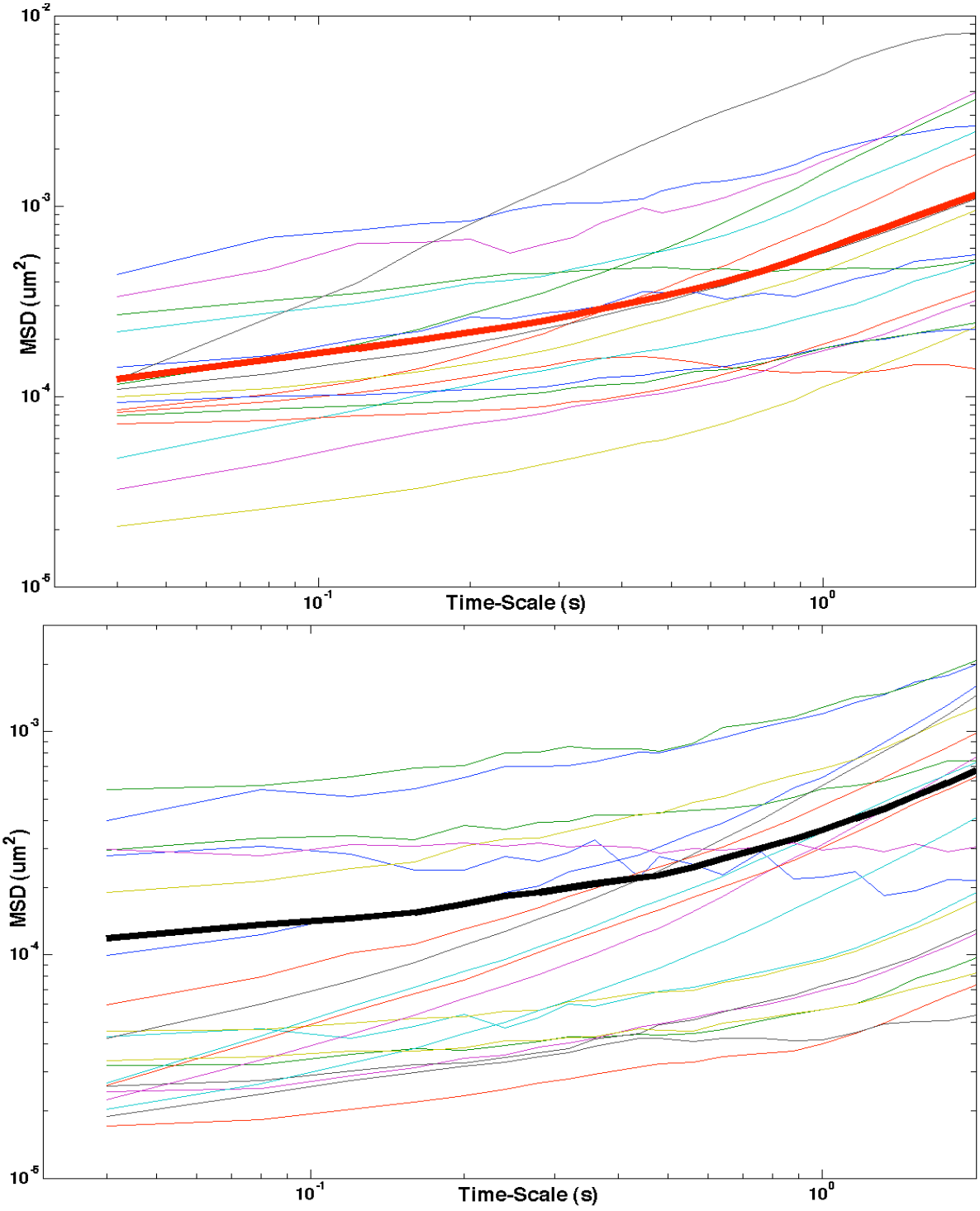

Figure 0.15: Individual MSD for particles tracked in cells at 9 hours (top) and 12 hours (bottom). The thick solid line represents the ensemble average of all MSDs.

The complex shear modulus is then computed from all four data points and plotted on a log-log graph against frequency (Figure 4.16). A frequency point, 3 rad/s, is chosen somewhat in the middle of the frequency range, away from frequency edges to avoid truncation errors as discussed in the method section. The elastic and viscous modulus are plotted against all four time points in Figure 4.17 for this specific frequency point.

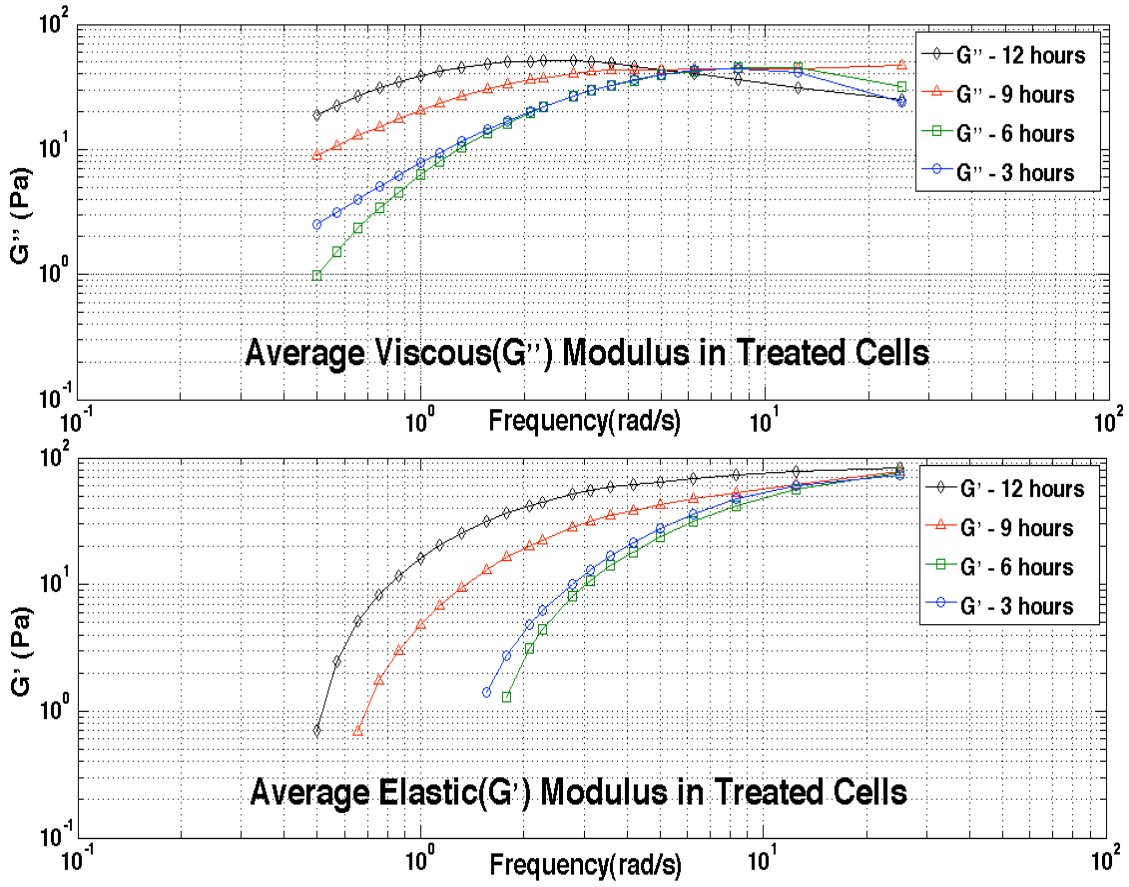

Figure 0.16: Elastic and viscous modulus change over all four time points of cisplatin treated cells. Modulus is computed using the Generalized Stokes-Einstein equation. An obvious increase is observed in the elastic and viscous modulus at frequencies below 25 rad/s and 5 rad/s respectively.

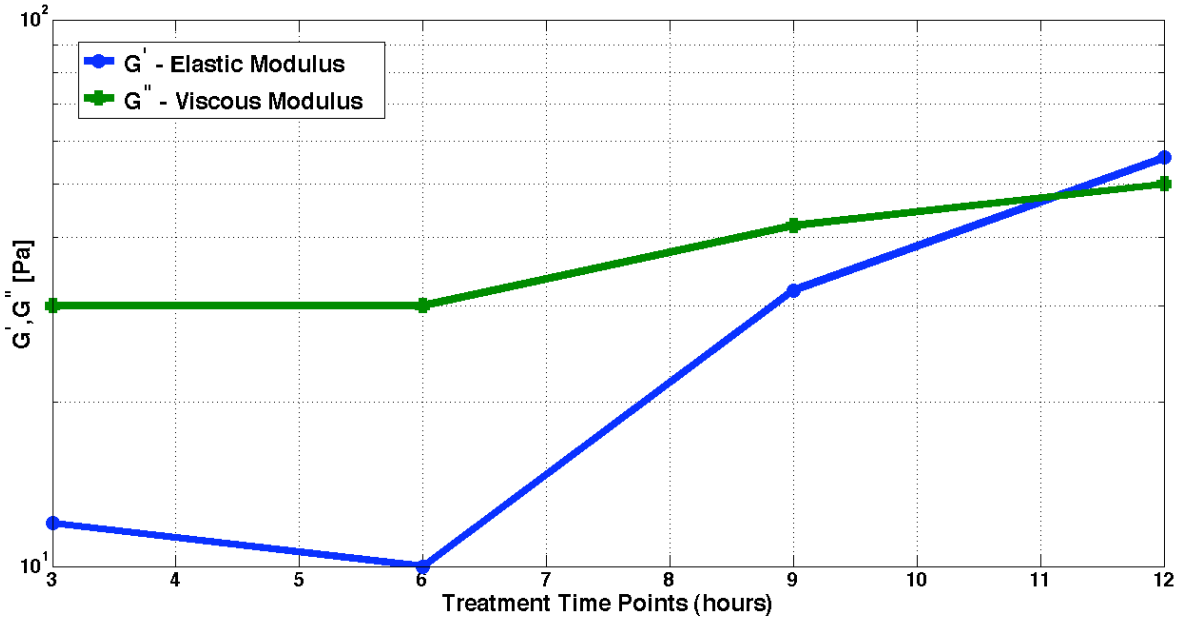

Figure 0.17: Viscous and Elastic Modulus at all four time points computed at ω = 3 rad/s as PC3 cells are undergoing treatment. The figure shows an increase in both moduli after the 6-hour mark. 3 rad/s was chosen to avoid frequency extrema.

4.2 Discussion

4.2.1 Glycerol

Overall, glycerol experiments showed that our system can measure the viscosity of Newtonian fluids with some limitations as described below. The first experiment was performed to observe the effects of bead concentrations on the MSD. It was concluded that the bead concentration does not affect the computed MSD within the time scales used (Figure 4.2). The highest bead concentration (28.8 x 10^9 particles/ml) was used for all remaining glycerol analysis and guar experiments. As expected, the MSD for each of the glycerol concentrations differed in magnitude but maintained α=1 over all time scales used. This signifies that PTM can measure variations in viscosities in a system such as a Newtonian fluid.

The complex shear modulus was extracted from the MSD where only the viscous modulus was available. The viscosities were computed from the viscous modulus and compared to literature values in Table 1. Agreement to within 10% was observed at the two lower glycerol concentrations. The agreement at 70% and 90% concentrations was lower. Deviations are assumed to be caused by glycerol concentration and temperature uncertainty.

Uncertainty in the concentrations produced during glycerol preparation are due to pipette volume uncertainty and difficulties encountered while transferring glycerol from one container to another (glycerol is a very thick substance). The uncertainty in volume dispersed by pipettes was calculated to be ~0.05ml. The thickness of the glycerol (due to its viscous nature) makes it difficult to transfer it from one container to another, adding further error to the final concentration. Uncertainties due to concentration errors are estimated to be approximately ±5%. From Figure 4.18, one can notice that a 5% deviation in the concentration at lower values results in a small deviation in corresponding viscosities while at higher concentrations, such an error leads to a large deviation in the viscosity (e.g. the true viscosity can range from 299 to 69 cP at 90% glycerol with an uncertainty of ±5%). Therefore the deviations in Table 1 can be partially explained by uncertainties in this measurement.

Similarly, temperature variations tend to cause large deviations in viscosity, especially at low temperatures. Figure 4.18 is a plot of the viscosities of 90% glycerol as a function of temperature. As our experiments were done at room temperature (25^{o}C with an estimated error of $\pm 1^{o}$C) it was estimated that the true viscosity measurement could lie anywhere between 141.5 and 163.1 cP.

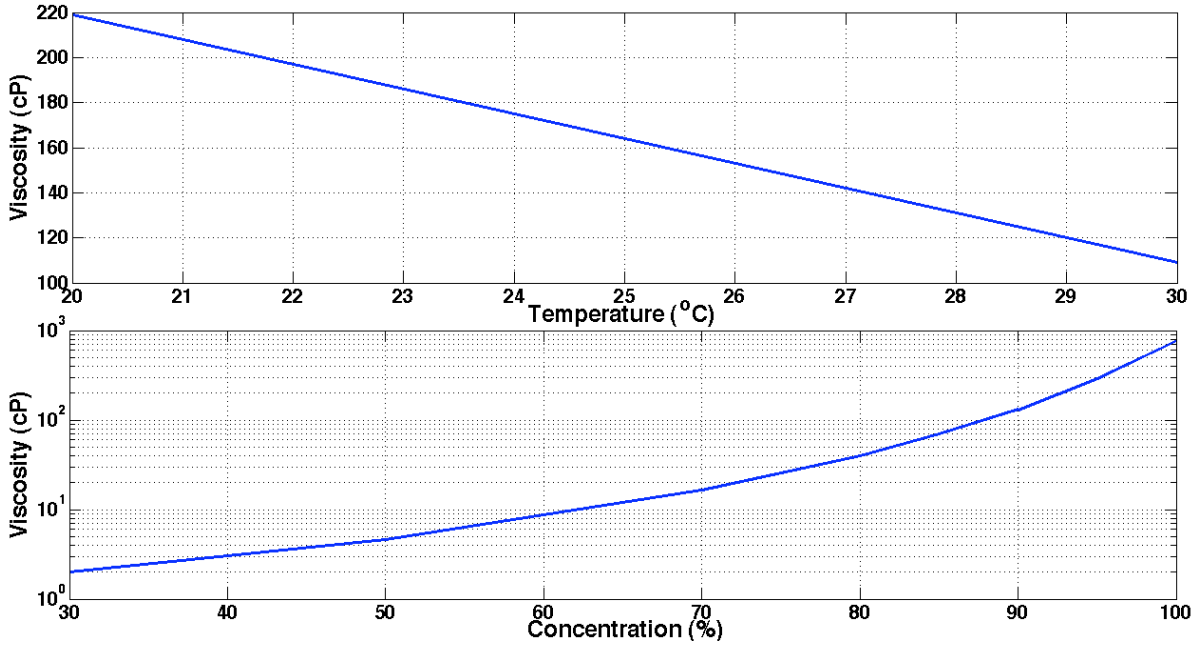

Figure 0.18: The top plot is the viscosity as a function of temperature for 90% glycerol and the bottom plot is the viscosity as a function of glycerol concentration at 25°C. Known literature measurements were used to generate these plots.

It is expected that the TPM MSD will match the PTM MSD for a homogeneous solution such as glycerol. In Figure 4.5, it is shown that the TPM MSD computed matched well the PTM MSD for the 90% glycerol concentration. A good match was also observed at other concentrations for lower time-scales. As some tracers remain in the focal plain longer than others, the number of available points to compute the mechanical properties decreases as the time-scale increases. Typically, this yields higher uncertainties and greater error at higher time-scales, but in Figure 4.5, a consistent over-estimation trend of the MSD is observed, which indicates that there may be another source of error affecting the TPM MSD.

4.2.2 Guar

From Figures 4.8, one can conclude that PTM is able to measure the elastic and viscous component of a viscoelastic system such as guar. Furthermore, the viscous and elastic modulus measured by PTM increases with increasing guar concentration, which indicates that our system is also able to measure changes in viscoelasticity. As expected, the range of magnitudes and slopes of individual MSDs various much more than that of glycerol (Figures 4.3 and 4.4 and Figure 4.7). This is because, unlike a homogeneous liquid such as glycerol, guar contains small pores of different sizes and varying mechanical properties. Each particle will then measure only local mechanical properties.

Figure 4.9 shows the PTM and TPM MSD for the 0.25% guar solution. As expected in a heterogeneous system, the two MSDs do not match. This indicates that the particles are much smaller than the length scale of heterogeneity and will therefore measure local mechanical properties only in the PTM MSD (from which G' and G" are computed in Figure 4.10). Theoretically, the TPM MSD should yield a shear modulus representative of the guar sample as a whole. The TPM shear modulus is then expected to match the bulk modulus measured with a rheometer.

Figure 4.10 shows that the TPM complex shear modulus matches more closely the mechanical properties of guar measured with a rheometer than those measured using only PTM. Nevertheless, deviations are still observed especially at the lower frequencies, indicating that TPM technique needs improvement.

4.2.3 Cells

In Figure 4.11, images at the 3 and 6 hour time points do not display significant cell morphology change, while images at the 9 and 12 hour points show signs of apoptosis (blebbing, shrinkage, nuclear condensation and morphology changes). Our study was aimed at better understanding changes in the mechanical properties of cells undergoing apoptosis, i.e. whether the cytoplasm becomes stiffer or softer as a function of treatment.

Two example tracks are displayed in Figure 4.12 at the 3 and 12-hour points. It is observed that the overall displacement decreases at the 12-hour point relative to the 3-hour point. This is a clear indication that the medium surrounding particles is stiffening, as it confines the particles to smaller movements.

Figure 4.13 clearly shows a decrease in the amplitude of the MSD and a change of slope in the MSD at times greater than 6 hours further indicating the stiffening of the cells as the apoptosis process is activated. The decrease in the slope of the MSD is a sign of an increase in the elastic nature of the system. One can observe in Figure 4.14 and 4.15 a similar trend observed with guar, where the individual MSDs have great variability in the distribution of slopes. As discussed in chapter 1, cells are extremely heterogeneous and so every particle will express a different MSD depending on its location in the cell.

Figure 4.17 shows the viscous and elastic modulus at 3 rad/s at four time points after treatment. This frequency was chosen to avoid errors occurring at the edges of the plots in Figure 4.16 due to truncation. It is observed that there is no significant change in the moduli at the 3 and 6hour points. A large increase of ~ 40 Pa (a 400% increase) in magnitude is

recorded for the elastic modulus while a smaller, yet present, increase in the viscous modulus of ~20 Pa (a 66% increase) is observed.

PTM measurements made on treated cells are averaged over many cells and at various locations within the cell itself. It is clear from these measurements that apoptosis causes cells to become more elastic and viscous over time. One would though expect an increase in ultrasound backscatter & attenuation. This is what is also seen experimentally (Brand *et al.,* 2008). This is the first time that PTM is shown to measure changes in mechanical properties of apoptotic cells. Demonstrating that cells become stiffer throughout the apoptosis process signifies that the observed HFUS backscatter measurements (discussed in chapter 1) are most probably due to this stiffening of the cell.

Chapter 5

Conclusion & Future Work

5.1 Conclusions

I have developed Intracellular Particle Tracking Microrheology to be used for studying the mechanical properties of cells undergoing apoptosis. I have further shown that PTM can be used to detect and provide quantitative estimates of the changing mechanical properties of treated cells.

My experiments involved embedding fluorescent particles in systems of interest and making videos of the random walk of these particles induced by the thermal energy of the system. MATLAB software was then used to track particles, from which I could then compute the MSD of each individual particle. An ensemble-averaged MSD calculated as a function of different time-scales could then be used to extract mechanical properties of the system. Furthermore, the slope of the MSD could be used to understand properties of the system surrounding the particles.

It was important to first validate our PTM set up. Various glycerol and guar concentrations were used to confirm that our system could indeed measure mechanical properties. Furthermore, attempts to quantify measurements of the viscous and elastic components of both glycerol and guar found that PTM can accurately measure the viscosities of glycerol to within 22%, but that it cannot do so for measurements of the viscous and elastic modulus, for both PTM and TPM, in a solution of 0.25% guar. For glycerol, a large

part of the uncertainty relates to the inaccurate measurement of small volumes & the lack of detailed knowledge of the temperature distribution. For guar, PTM measurements reflect only local mechanical properties, which cannot be validated.

Initial attempts to develop a technique known as Two-Point Particle Tracking Microrheology are presented in this work. As expected, PTM and TPM MSDs agree for a homogeneous material such as glycerol, while two distinct MSDs (one for PTM and one for TPM) are observed in materials that are heterogeneous on the length scale of the particle-probe. Indeed the complex shear modulus in guar computed from TPM was closer to the rheometer measure values, but deviations indicate that the technique needs further refinement before it can be applied to cells.

PC3 cells were used for PTM cell experiments. These cells were microinjected with carbohydroxilated 0.2 μm particles and then treated with cisplatin to induce apoptosis. It was observed that the MSD of a particle in a 1000 frame video became much smaller with time, as apoptosis was induced. This indicated stiffening of the intracellular environment in which the bead was submerged. The MSD was shown to decrease both in magnitude and slope over time. At a frequency of 3 rad/s, the elastic modulus increases by 50 Pa while the viscous modulus increases by 20 Pa.

5.2 Future Work

PTM is a powerful tool, revealing much about the mechanical properties of complex soft materials (Waigh, 2005). An important future step will be to consider individual particle's movements and how the MSD changes at various spatial locations within the cell. By studying the tracks of individual tracers embedded in a material of interest using statistical or

mathematical tools, particles that may be affected by active motors present in the cell can be excluded from the analysis. Furthermore, this would shed light on the mechanics and nature of distinct regions within the cytoplasm and the cell. A mechanical mapping of a cell at different time points after treatment could also be developed. To do so, it will be essential to develop mathematical tools such as those developed for non-biological materials by (Valentine et al., 2006). Developing such tools could also help characterize and further identify spurious tracks, which could then be eliminated from the analysis.

An important question, which could be tackled, is: which part of the cell is predominantly responsible in the backscatter observed when apoptotic cells are imaged using HFUS? As PTM has been used in the past to study the mechanical properties of the nucleus (Tseng et al., 2006), it is then possible to refine our set up to study the viscoelasticity of cell nucleus undergoing apoptosis. This will require improving on the microinjection method to be able to reach the nucleus and inject particles.

Both of the above mentioned future work could be used to study how the mechanical properties of cell change immediately before obvious apoptosis characteristics are observed. These properties can then be correlated with the HFUS backscatter, allowing the detection of cells that are about to undergo apoptosis. As new methods to immobilize non-adherent cells are now reported (Rosenbluth et al., 2006), these cells could then be microinjected and would make an interesting study with PTM.

It will be important to further test and refine TPM. To do so, further experiments on viscoelastic phantoms, where the length scale of heterogeneity is much greater than the radius of tracers, can be conducted and compared to known bulk measurements (from a

rheometer). These results can then be used to conduct a study on how to best optimize parameters (described in the methodology section) associated with the technique. TPM cell experiments will help yield more precise measurements of bulk viscoelasticity measurements of cells, which can then be used in numerical models. Nevertheless, TPM is limited by the high amount of data and computational power needed to obtain viscoelastic measurements. Although this may be easier to overcome in materials such as glycerol and guar, the small physical size of cells makes it difficult to collect videos with a high number of particles. One way to overcome this would be to improve on the microinjection technique as to insure a maximum number of particles is injected and that more cells remain viable after injection. This may then allow to capture more particle tracks for analysis. This will provide more tracks for analysis. A study should also be conducted to determine the number of particles that a cell can hold without affecting its mechanical properties.

An advantage to TPM is its ability to extract mechanical properties by tracking endogenous particles (i.e. lipid granules) already present in the cell, eliminating the need of microinjection and the introduction of particles, which may in turn disturb the cell's condition (no known study has been conducted on the effects of microinjection and the introduction of particles within the cell). The cross correlation of bead pairs eliminates motion that is not caused by the random fluctuation the material inside the cell.

Finally, TPM and PTM are both limited by a frequency range of viscoelastic measurements as described in the theory section. In order to further correlate and understand the mechanical properties of cells at higher frequencies (near the MHz frequencies utilized in the HFUS experiments), it will be important to develop methods to measure or scale cell

mechanics to higher frequencies. Gisler *et al.,* (1999) & Fabri *et al.,* (2001) have developed methods to scale low frequency microrheology measurements to higher frequencies, but none have been able to overcome the 100 kHz boundary set by inertial effects yet.

Appendix A

The following is step-by-step instructions on how the cells were microinjected.

1. 10x magnification is first used to focus on cell cluster

2. The pipette is brought over illuminated area under microscope and slightly dipped in cell medium.

3. Focus is then raised a few turns over the cell level.

4. The pipette is gently moved (on x-y axis only) within illuminated area until its shadow is observed, at which the tip of the pipette is brought into focus. The pipette is then centered in the field of view.

5. The focal plane is lowered again slightly over cells so that the cells are seen but are slightly out of focus. Pipette is then lowered until tip is in focus.

6. The objective lens is changed to the 40x magnification.

7. Cells are brought into focus and the pipette is gently lowered until its shadow is seen. At this point, the focal plane can be set on the pipette and turning fluorescence on can test the injection pressure. The pressure is adjusted accordingly.

8. If pipette is clogged or no particles are being released, focus back on the cells and lower pipette gently while moving it side ways until it touches the bottom of the well. At this point, the tip will chip slightly and particles should start ejecting. Make sure no cells are below the pipette while lowering.

9. Raise pipette again and bring it over a cell. Set a small constant positive pressure and start lowering the pipette over the cell.

10. Aim to lower the pipette over the nucleus of the cell until a slight deformation in the membrane of the cell is observed, at this time press the inject button and very gently tap the microscope or the table to cause the pipette to penetrate the cell. If pressure is too high, the cell will fill up with air quickly and burst, if the pressure is too low, nothing will be observed. A good pressure will cause a small wave of air to travel in the cell. Once injection is done, immediately remove the pipette from the cell. Injection shouldn't last more than 3-4 seconds.

11. Repeat injection steps for other cells. If pipette is clogged, try to apply a clear pressure or bring the pipette outside the well and bring it back in. If it is still clogged, chip the tip some more.

Bibliography

Brown, R. (1828). A brief account of microscopical observations made in the months of June, July and August, 1827, on the particles contained in the pollen of plants; and on the general existence of active molecules in organic and inorganic bodies. *Phil.Mag,* 4, 161.

Chen, D., Weeks, E., Crocker, J., Islam, M., Verma, R., Gruber, J. et al. (2003). Rheological Microscopy: Local Mechanical Properties from Microrheology. *Physical Review Letters,* 90(10), 108301.

Crocker, J. C., & Grier, D. G. (1996). Methods of Digital Video Microscopy for Colloidal Studies. *Journal of colloid and interface science,* 179(1), 298-310.

Crocker, J., Valentine, M., Weeks, E., Gisler, T., Kaplan, P., Yodh, A. et al. (2000). Two-Point Microrheology of Inhomogeneous Soft Materials. *Physical Review Letters,* 85(4), 888-891.

Crocker, J. C., & Hoffman, B. D. (2007a). Multiple-particle tracking and two-point microrheology in cells. *Methods in cell biology,* 83, 141-178.

Czarnota, G. J., Kolios, M. C., Abraham, J., Portnoy, M., Ottensmeyer, F. P., Hunt, J. W. et al. (1999). Ultrasound imaging of apoptosis: high-resolution non-invasive monitoring of programmed cell death in vitro, in situ and in vivo. *British journal of cancer,* 81(3), 520-527.

Czarnota, G. J., Kolios, M. C., Vaziri, H., Benchimol, S., Ottensmeyer, F. P., Sherar, M. D. et al. (1997). Ultrasonic biomicroscopy of viable, dead and apoptotic cells. *Ultrasound in medicine & biology,* 23(6), 961-965.

Daniels, B. R., Masi, B. C., & Wirtz, D. (2006). Probing single-cell micromechanics in vivo: the microrheology of C. elegans developing embryos. *Biophysical journal,* 90(12), 4712-4719.

Dawson, M., Wirtz, D., & Hanes, J. (2003). Enhanced viscoelasticity of human cystic fibrotic sputum correlates with increasing microheterogeneity in particle transport. *The Journal of biological chemistry,* 278(50), 50393-50401.

Einstein, A. (1956). *Investigations on the theory of the Brownian movement.* New York, N.Y.: Dover.

Falou, O., Kumaradas, J. C., & Kolios, M. C. (2006). Modeling Acoustic Wave Scattering from Cells and Microbubbles. *Proceedings of Comsol Users Conference, Boston, USA, .*

Fabry B., Maksym G., Butler J.P., Glogauer M., Navajas D., and Fredberg J.J. (2001). Scaling the microrheology of living cells. *Phys. Rev. Lett. 87, 148102*

Fung, Y. C. (1993). *Biomechanics: mechanical properties of living tissues.* (2nd ed. ed.). New York: Springer-Verlag.

Gardel, M., Valentine, M., & Weitz, D. (2005). Microrheology. *Microscale Diagnostic Techniques.Heidelberg, Springer-Verlag Berlin Heidelberg, 2005.,* , 1-49.

Gardel, M. L., Nakamura, F., Hartwig, J., Crocker, J. C., Stossel, T. P., & Weitz, D. A. (2006). Stress-dependent elasticity of composite actin networks as a model for cell behavior. *Physical Review Letters,* 96(8), 088102.

Gisler, T., & Weitz, D. (1999). Scaling of the Microrheology of Semidilute F-Actin Solutions. *Physical Review Letters,* 82(7), 1606-1609.

Gordon, V. D., Valentine, M. T., Gardel, M. L., Andor-Ardo, D., Dennison, S., Bogdanov, A. A. et al. (2003). Measuring the mechanical stress induced by an expanding multicellular tumor system: a case study. *Experimental cell research,* 289(1), 58-66.

Haw, M. D. (2002). Colloidal suspensions, Brownian motion, molecular reality: a short history. *Journal of Physics: Condensed Matter,* 14(33), 7769-7779. from http://stacks.iop.org/0953-8984/14/7769.

Hoffman, B. D., Massiera, G., Van Citters, K. M., & Crocker, J. C. (2006). The consensus mechanics of cultured mammalian cells. *Proceedings of the National Academy of Sciences,* 103(27), 10259.

Humphrey, J. D. (2004). *An introduction to biomechanics: solids and fluids, analysis and design.* New York: Springer.

Jiang, G., Huang, A. H., Cai, Y., Tanase, M., & Sheetz, M. P. (2006). Rigidity sensing at the leading edge through avb3 Integrins and RPTPa. *Biophys J,* 90, 1804-1809.

Kasza, K. E., Rowat, A. C., Liu, J., Angelini, T. E., Brangwynne, C. P., Koenderink, G. H. et al. (2007). The cell as a material. *Current opinion in cell biology,* 19(1), 101-107.

Kerr, J. F., Wyllie, A. H., & Currie, A. R. (1972). Apoptosis: a basic biological phenomenon with wide-ranging implications in tissue kinetics. *British journal of cancer,* 26(4), 239-257.

Kole, T. P., Tseng, Y., Jiang, I., Katz, J. L., & Wirtz, D. (2005). Intracellular Mechanics of Migrating Fibroblasts. *Molecular biology of the cell,* 16(1), 328-338.

Kole, T. P., Tseng, Y., & Wirtz, D. (2004). Intracellular microrheology as a tool for the measurement of the local mechanical properties of live cells. *Methods in cell biology,* 78, 45-64.

Kolios, M., Czarnota, G., Worthington, A., Giles, A., Tunis, A., & Sherar, M. (2004). Towards understanding the nature of high frequency backscatter from cells and tissues: an investigation of backscatter power spectra from different concentrations of cells of different sizes. *Ultrasonics Symposium, 2004 IEEE,* 1.

Kolios, M. C., Czarnota, G. J., Lee, M., Hunt, J. W., & Sherar, M. D. (2002). Ultrasonic spectral parameter characterization of apoptosis. *Ultrasound in medicine & biology,* 28(5), 589-597.

Lau, A., Hoffman, B., Davies, A., Crocker, J., & Lubensky, T. (2003). Microrheology, Stress Fluctuations, and Active Behavior of Living Cells. *Physical Review Letters,* 91(19), 198101.

Levine, A. J., & Lubensky, T. (2000). One-and Two-Particle Microrheology. *Physical Review Letters,* 85(8), 1774-1777.

Lim, C. T., Zhou, E. H., & Quek, S. T. (2006). Mechanical models for living cells--a review. *Journal of Biomechanics,* 39(2), 195-216.

Mason, T. G. (2000). Estimating the viscoelastic moduli of complex fluids using the generalized Stokes-Einstein equation. *Rheologica Acta,* 39(4), 371-378.

Mason, T., Gisler, T., Kroy, K., Frey, E., & Weitz, D. (2000). Rheology of F-actin solutions determined from thermally driven tracer motion. *Journal of Rheology,* 44, 917.

Mason, T. G., Ganesan, K., van Zanten, J. H., Wirtz, D., & Kuo, S. C. (1997). Particle Tracking Microrheology of Complex Fluids. *Physical Review Letters,* 79(17), 3282-3285. from 10.1103/PhysRevLett.79.3282.

Mason, T. G., Gang, H., & Weitz, D. A. (1997). Diffusing-wave-spectroscopy measurements of viscoelasticity of complex fluids. *Journal of the Optical Society of America A-Optics Image Science and Vision,* 14(1), 139-149.

Mason, T. G., & Weitz, D. A. (1995). Optical Measurements of Frequency-Dependent Linear Viscoelastic Moduli of Complex Fluids. *Physical Review Letters,* 74(7), 1250-1253. from 10.1103/PhysRevLett.74.1250.

Oppong, F. K. (2005). *Probing the microstructure of yield-stress fluids using multiple particle tracking.* Doctoral dissertation, Memorial University of Newfoundland (Canada).

Pai, V. B., & Khan, S. A. (2002). Gelation and rheology of xanthan/enzyme-modified guar blends. *Carbohydrate Polymers,* 49(2), 207-216.

Panorchan, P., Lee, J. S., Daniels, B. R., Kole, T. P., Tseng, Y., & Wirtz, D. (2007). Probing cellular mechanical responses to stimuli using ballistic intracellular nanorheology. *Methods in cell biology,* 83, 115-140.

Pelling, A. E., & Horton, M. A. (2008). An historical perspective on cell mechanics. *Pflugers Archiv : European journal of physiology,* 456(1), 3-12.

Phan-Thien, N. (2002). *Understanding viscoelasticity: basics of rheology.* New York: Springer.

Pullman, B., (1998). The atom in the history of human thought, Oxford, UK: Oxford University Press, p. 403

Sherar, M., & Foster, F. (1987). A 100 MHZ PVDF Ultrasound Microscope With Biological Applications.

Tseng, Y., Kole, T. P., Lee, S. H. J., & Wirtz, D. (2002). Local dynamics and viscoelastic properties of cell biological systems. *Current Opinion in Colloid & Interface Science,* 7(3-4), 210-217.

Tseng, Y., Kole, T. P., & Wirtz, D. (2002). Micromechanical Mapping of Live Cells by Multiple-Particle-Tracking Microrheology. *Biophysical journal,* 83(6), 3162-3176.

Tseng, Y., Lee, J. S., Kole, T. P., Jiang, I., & Wirtz, D. (2004). Micro-organization and visco-elasticity of the interphase nucleus revealed by particle nanotracking. *Journal of cell science,* 117(Pt 10), 2159-2167.

Valentine, M., Kaplan, P., Thota, D., Crocker, J., Gisler, T., Prud'homme, R. et al. (2001). Investigating the microenvironments of inhomogeneous soft materials with multiple particle tracking. *Physical Review E,* 64(6), 61506.

Valentine, M., Perlman, Z., Gardel, M., Shin, J., Matsudaira, P., Mitchison, T. et al. (2004). Colloid Surface Chemistry Critically Affects Multiple Particle Tracking Measurements of Biomaterials. *Biophysical journal,* 86(6), 4004-4014.

Valentine, M. T. (2003). *Mechanical and microstructural properties of biological materials*. Doctoral dissertation, Harvard University.

Van Citters, K. M., Hoffman, B. D., Massiera, G., & Crocker, J. C. (2006). The role of F-actin and myosin in epithelial cell rheology. *Biophysical journal,* 91(10), 3946-3956.

Viigipuu, K., & Kallio, P. (2004). Microinjection of living adherent cells by using a semi-automatic microinjection system. *Alternatives to Laboratory Animals : ATLA,* 32(4), 417-423.

Waigh, T. A. (2005). Microrheology of complex fluids. *Reports on Progress in Physics,* 68(3), 685-742.

Weihs, D., Mason, T. G., & Teitell, M. A. (2006). Bio-microrheology: a frontier in microrheology. *Biophysical journal,* 91(11), 4296-4305.

Xu, J., Palmer, A., & Wirtz, D. (1998). Rheology and microrheology of semiflexible polymer solutions: actin filament networks. *Macromolecules,* 31(19), 6486-6492.